NATIONAL TECHNICAL UNIVERSITY OF ATHENS
School of Civil Engineering
Institute of Steel Structures

Analysis and design of a telecommunication steel tower strengthened with FRP plates

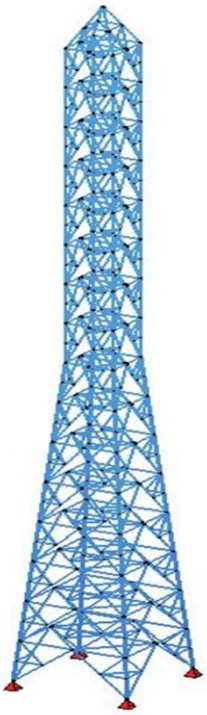

MASTER THESIS

Konstantinos V. Vlachakis

Supervisor: Ioannis Vayas

Athens, October 2018

EMK ME 2018/15

Βλαχάκης Β. Κ.. (2018).
Ανάλυση και σχεδιασμός μεταλλικού ιστού τηλεπικοινωνιών ενισχυμένου με ελάσματα από ινοπλισμένα πολυμερή (FRP)
Μεταπτυχιακή Εργασία ΕΜΚ ΜΕ 2018/15
Εργαστήριο Μεταλλικών Κατασκευών, Εθνικό Μετσόβιο Πολυτεχνείο, Αθήνα.

Vlachakis V. K. (2018).
Analysis and design of a telecommunication steel tower strengthened with FRP plates
Master Thesis EMK ME 2018/15
Institute of Steel Structures, National Technical University of Athens, Greece

Contents

NATIONAL TECHNICAL UNIVERSITY OF ATHENS
SCHOOL OF CIVIL ENGINEERING
INSTITUTE OF STEEL STRUCTURES

MASTER THESIS
EMK ME 2018/15

Analysis and design of a telecommunication steel tower strengthened with FRP plates

Vlachakis V. K. (supervised by Vayas I.)

Abstract

Telecommunication lattice towers are probable the most common type of tower used for telecommunication purposes. They have many advantages like the easy on-site transport and erection due to the use of angle sections. However, over the last years several towers' failures have occurred due to severe weather conditions. Also, telecommunication market needs have a tremendous increase, more and larger antennas need to be placed on existing towers. Based on the above it seems that in many cases strengthening of existing towers is unavoidable. In the current practice, replacing the leg member with a larger angle is not feasible, so a second angle is usually inserted and connected with the existing section to form a built-up member in a star-battened configuration. This common strengthening method has some significant disadvantages, with most important the increasement of the structural weight and the area swept by the wind, and therefore the wind forces. An alternative strengthening method is introduced in this thesis, by which the legs or braces are strengthened using Carbon Fiber Polymer plates (CFRP).

Because both literature and experimental test on steel sections strengthened with CFRP plates are limited, it is needed to be executed several experimental tests on steel sections strengthened with CFRP plates. For this purpose, three tests are executed on such specimens, one tensile test and two four-point bending tests, in order to estimate the response and the strength of strengthened steel members. Besides the tests, analytical calculations based on two different methods and numerical analyses using Finite elements software are made. As it is concluded, CFRP strengthening increased tensile and bending capacity of the steel plate almost 5 times, independently if the CFRP was in the tension or in compression side. That means that CFRP plates have also a large strength on compression stresses.

Using the results of the experimental tests, the design of a telecommunication tower strengthened with CFRP plates follows. At first, an evaluation of a typical existing tower is made. As it is proved the existing tower cannot bear some typical loads in order to fulfil codes' requirements and future telecommunication needs. Both towers' legs and braces are overloaded almost all over the height of the tower.

In the alternative strengthening method CFRP plates are bonded only to members that fail. This application doesn't increase the wind loads since the reference wind area is the same and also there is no increase in dead loads. Nonlinear analysis and then structural design is executed. As it is concluded, finally, the strengthening of an existing telecommunication tower using CFRP plates is a possible solution, that may be very effective and has certain advantages comparing with the conventional strengthening method. It is obvious, that more research need to be done so that this alternative method can be feasible.

1 General information

1.1 Typical lattice telecommunication towers

1.1.1 General

A large number of lattice towers exist and are being built worldwide for telecommunication purposes. This is due to the fact that such towers are very often installed in mountainous terrain with very limited access to heavy vehicles and cranes. Accordingly, a lattice tower structural system, which can be transported and erected by light machinery and equipment, is almost the only possible solution. Theoretically, lattice towers need more ground space compared to cylindrical, octagonal or similar shell-type systems. However, ground space is plentifully available in remote places outside the densely populated regions. In conclusion, it may be argued that besides general structural engineering purposes, lattice towers are and will remain the main structural system for telecommunication towers.

The members of such towers are frequently composed of equal leg angle sections that are often preferred to tubular sections due to their easier connection that results in a simpler on-site erection and easy transport, a requirement set by most telecommunication or power providers. Also, angles are not susceptible to the well-known problems, such as the appearance of cracks after hot dip galvanizing, unlike other types of open or closed cross sections. Equal angle sections are widely used today as legs or bracing members in free standing lattice towers.

Angles sizes range from light to heavy sections with leg lengths up to 300 mm that are lately produced in Europe and are employed for towers with increased height. Appropriate long life corrosion protection is ensured with application of angles, since all angle sizes are fully amenable to hot dip galvanizing in contrast to several other types of open or closed sections. The tower members are entirely hot-dip-galvanized and for this purpose welding must be avoided and all connections must be done by hot-dip-galvanized bolts. Welding is allowed only for towers' footings construction, the sections of the climbing stair and the lightning arrester of the towers.

Lattice free-standing telecommunication towers are specifically provided for heights ranging from 20m to 80m. Towers are rated as "heavy" or "light", according to their design. More specifically, the basic difference between "heavy" and "light" is the bracing pattern. At a "heavy" type tower there is also a secondary vertical bracing system, which reduces the effective buckling length of the main braces and has as a result the increase of the tower's total load capacity.

The towers may be distinguished in the following main categories:

I. By plan:
- Square Lattice Towers
- Triangular Lattice Towers

II. By cross section type of members
- Lattice towers with tubular profile members
- Lattice towers with angles

Figure 1.1: Telecommunication towers

1.1.2 Square lattice towers

Square lattice towers are square in plan. They are composed of four legs connected by various types of bracings (Figure 1.2). Depending on the height of the tower, the legs may be inclined from the base to the top, may be vertical from the base to top, or may be inclined from the base up to a certain height and then continue vertical to the top. The primary bracing pattern may be either Λ-type, X-type or N-type. Primary bracing is complemented by secondary bracings in various patterns that reduce the buckling length of legs and primary bracing members.
The dimension of the square tower's base varies from 1.50m to 12.5m. The foundation of the structure is realized by a concrete slab C20/25 connecting the legs of the tower. At certain distances along the height of the tower, diaphragms are placed. At certain heights there are also resting platforms. The diaphragm types for square towers with angle members are indicatively shown in Figure 1.3. It consists of UPN or angle sections, forming a rectangular shape which inscribes a rotated square shape, also made of angle sections.

The most usual cross sections of the structural system are:

- Legs vary from L80.8 to L200.20
- Vertical main braces vary from L70.7 to L110.10
- Secondary bracing members vary from L25.5 to L55.5
- Horizontal members vary from UPN 80 to UPN 100
- Horizontal bracing members made of UPN and angle sections

All towers have:

- Vertical access stair, safety ring and devices against back fall
- Vertical holsters for feeders, electrical cables, night beacon and lightening system

Typically, there are at least 4 triple band antennas symmetrically installed at the upper part of the tower and parabolic antennas installed at various heights with diameters that vary from 0.3m to 3.2m

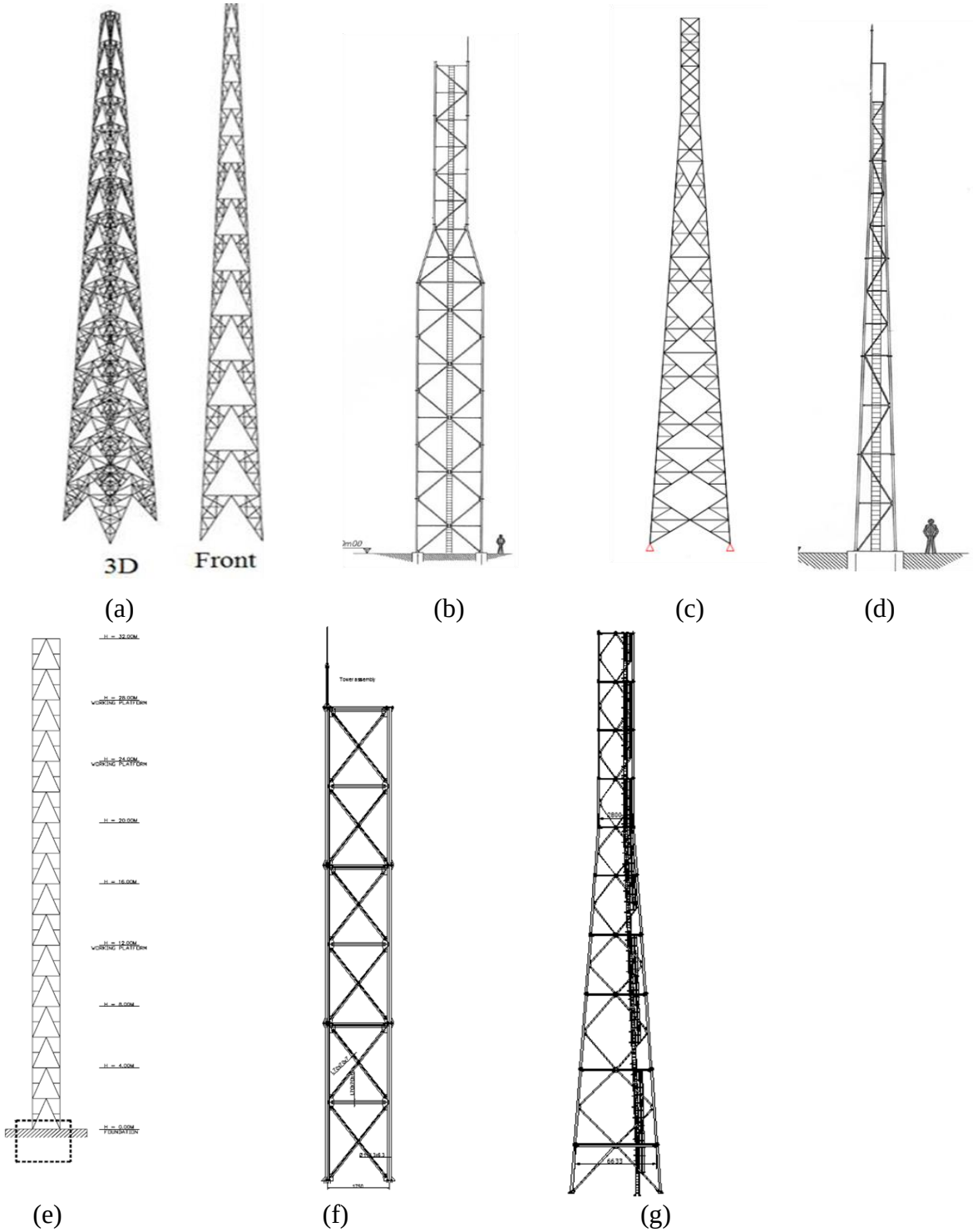

Figure 1.2: Square Lattice towers

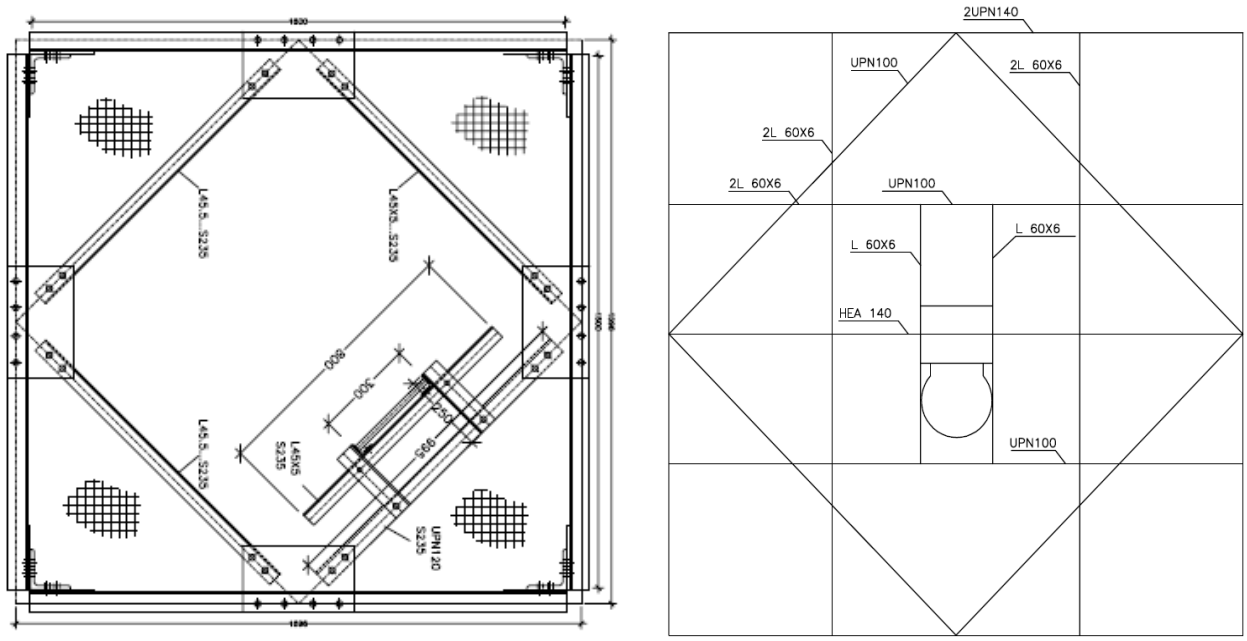

(a) (b)

Figure 1.3: Diaphragm types of square towers

1.1.3 Triangular lattice towers

Triangular lattice towers form an equilateral triangle shape in plan. They are composed of three legs connected at an angle of 120^0 by various types of bracing systems (Figure 1.4). The legs are usually inclined from the base to the top, but for short towers they may be vertical or be inclined up to a certain height and then continue vertical. The primary bracing pattern may be either Λ-type, X-type or N-type. Primary bracing is complemented by secondary bracings in various patterns to reduce the buckling length of legs and primary bracing members. Triangular towers are torsional stiffer than square towers. However, there is a restriction in the appropriate cross sections for leg members to tubular sections that is associated to more assembly effort. Alternatively, cross sections for legs may be special angle sections, in which the angle legs are not at a 90-degree angle but at a 60-degree angle. Such cross sections require special fabrication.

The diaphragm types for triangular lattice towers are shown in Figure 1.5, and consist of tubular sections forming a triangular shape. Inside this shape a second triangular shape formation is inscribed. The diaphragm's dimensions vary from 1.60m to 9m.

The tubular sections' diameters range between 42 mm and 127 mm and their thickness varies from 4 mm to 14 mm. The connection elements (flanges, angle brackets etc.) have a thickness between 5 mm and 16 mm

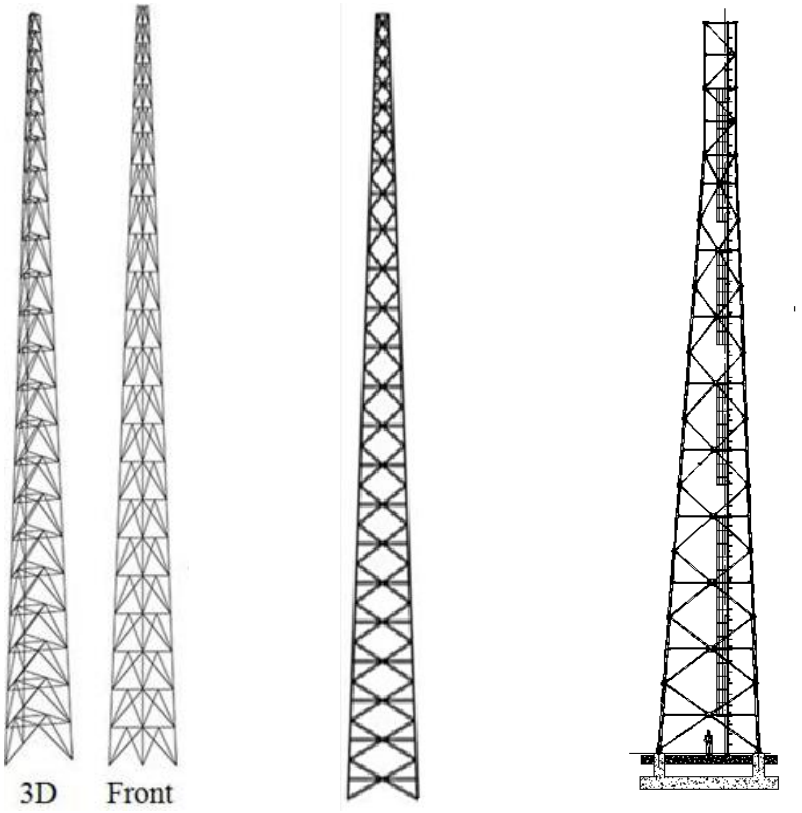

(a) (b) (c)

Figure 1.4: Triangular Lattice towers

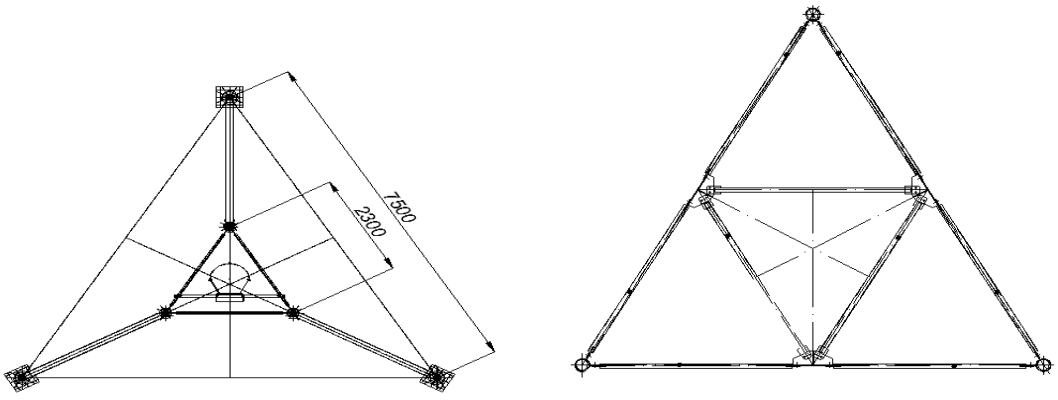

(a) (b)

Figure 1.5: Diaphragm types of triangular towers

1.2 Strengthening existing telecommunication lattice towers

1.2.1 Need for strengthening

Severe weather conditions combining low temperatures, snow and wind are often the governing loading condition. Wet snow accumulates in the form of ice on towers and antennas, adding to gravity loads, dramatically increasing wind drag and leading to tower collapse. This is the leading cause for tower collapses in operation, that have occurred on

several occasions. Based on that, evaluation of old or corroded towers is necessary to be executed in order to verify their bearing capacity.
In addition, code provisions have been evolved significantly and it is proved that latest provisions, especially those regarding calculation of wind and snow loading, are unfavorable and more conservative than the older ones, that were used for the design of telecommunication towers during previous decades. This means that the evaluation of existing old towers following the latest provisions would probably lead to the necessity of strengthening these towers.

Figure 1.6: Failure of telecommunication towers

Telecommunication towers constitute a special case due to the fact that wind loading frequently varies during their design life due to modifications, like the provision of more and larger antennas, so that gravity and especially wind loading increase. The communication industries have seen a tremendous development in last years which has resulted in new technologies. Future market needs indicate that more and quite larger triple band and parabolic antennas need to be placed on existing towers in order to fulfil new technology (5G) requirements and enhance the coverage area and network consistency. This may result also in a requirement for strengthening the structure of the tower in order to bear all the extra and future loads.

1.2.2 Conventional strengthening method

In the current practice, replacing the leg member with a larger angle is not feasible, thus, a second angle is usually inserted and connected with the existing section to form a built-up member. For ease of erection, a star battened configuration may be used, where the two angles are connected by pairs of battens in two perpendicular planes. (Figure 1.8). Braces are either strengthened in the same manner or the old section may be replaced by a larger angle section. Although this is the only feasible solution since it intervenes from outside the existing structure, this is not the best one from the structural point of view due to the fact that it increases the structural weight and the area swept by the wind, and therefore the wind forces. In addition, it results in a fixed degree of strengthening, independent on how much is required due to the application of the same angle profile as the existing one.

Strengthening existing tower members from angle sections using smaller angles than the existing ones may lead to substantial economic benefits which may be summarized to less weight, less area and accordingly less additional wind loading and less erection effort, but there are not code-supported recommendations for this design case. Subdividing the bracing patterns, to reduce the slenderness, is another option in towers where the original slenderness is very high.

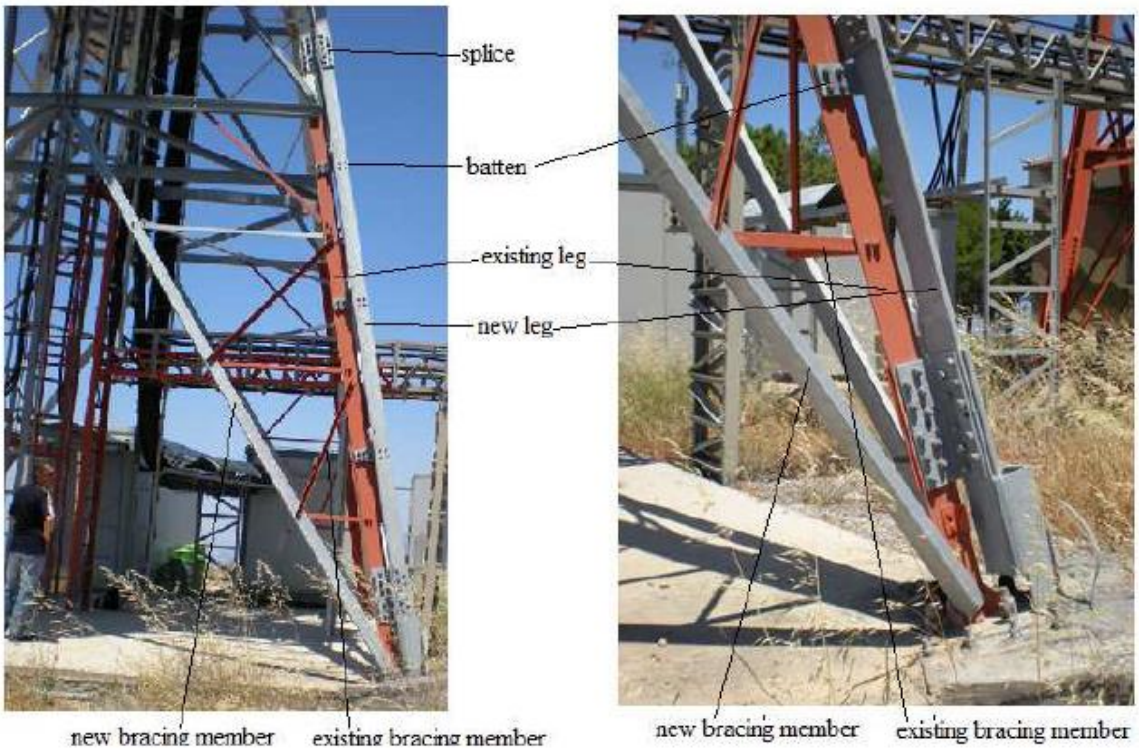

Figure 1.7: Strengthening of existing lattice tower

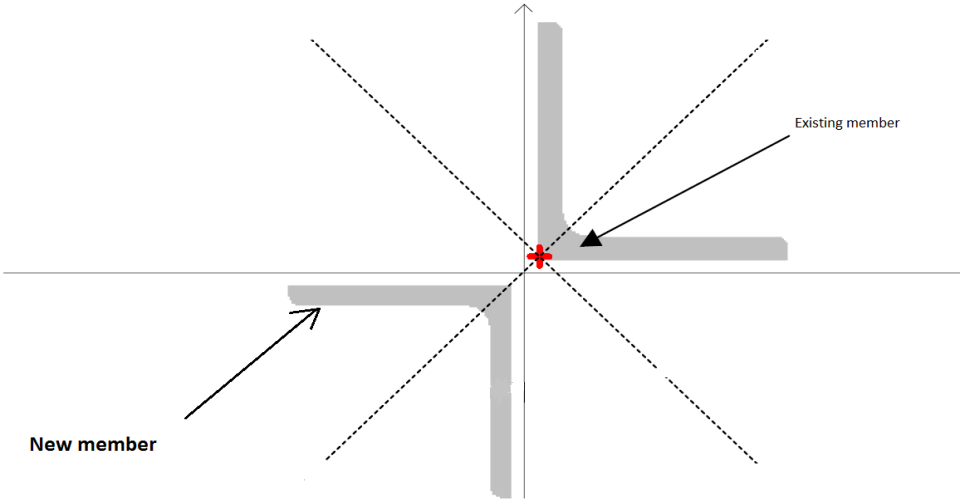

Figure 1.8: Star-battened configuration for legs

1.2.3 Strengthening using FRP plates

As an alternative to the previous conventional strengthening method, this thesis introduces a hybrid strengthening solution by which the tower members, whether legs or braces, are strengthened by fiber reinforced polymers (FRP) plates. The hybrid solution is expected to

be most advantageous from the structural and constructional point of view due to the combination of the following:
a) negligible increase of the reference wind area and therefore of the wind forces,
b) no increase of structural self-weight,
c) no need for exchange of brace profiles,
d) adjustment and fine tuning of the extent of strengthening to the design needs
e) great strength to corrosion and fatigue.

Although, the application of FRP strips is very common for rehabilitation and strengthening concrete structures, little research effort has been made internationally to strengthening of steel profiles with FRPs up to the present. It is therefore not surprising that, in contrast to reinforced concrete, practical applications for FRP-interventions in steel profiles are rather scarce and there exist no Codes or Recommendations at present at European level apart from a design guide [6]. Until now, FRP strips are usually used instead of FRP plates in steel structures and are applied mainly on strengthening steel pipes, bridges, trusses and transmission towers as shown in Figure 1.9. Using FRPs to enlarge the bending and compression capacity of steel sections was studied in [8]- [13]. Also, strengthening of angle section columns with FRPs was studied by a limited number of experiments at the Institute of Steel Structures, NTUA, [7]. (Figure 1.10).

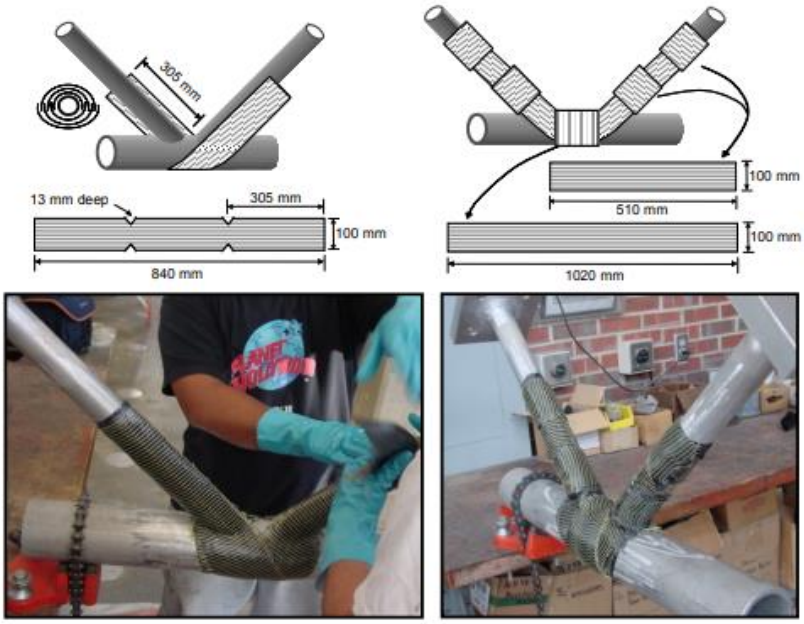

Figure 1.9: Strengthening of a truss joint using FRP strips

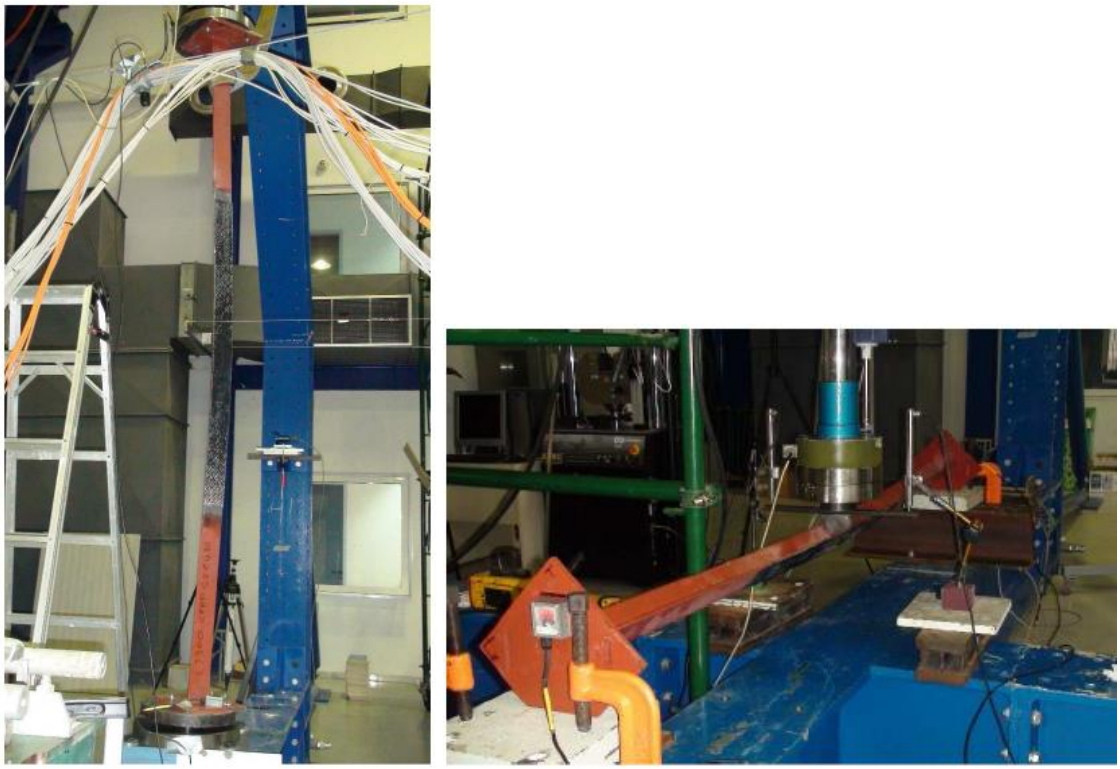

Figure 1.10: Tests on angle members strengthened with FRP strips

1.3 Fiber reinforced polymer material

1.3.1 Composite material

A Composite in engineering sense is any materials that have been physically assembled to form one single bulk without physical blending to foam a homogeneous material. The resulting material would still have components identifiable as the constituent of the different materials. One of the advantages of composite is that two or more materials could be combined to take advantage of the good characteristics of each of the materials. Usually, composite materials will consist of two separate components, the matrix and the filler. The matrix is the component that holds the filler together to form the bulk of the material. It usually consists of various epoxy type polymers, but other materials may be used, plastic for example. The filler is the material that has been impregnated in the matrix to lend its advantage (usually strength) to the composite. The fillers can be of any material such as carbon fiber, glass bead, sand, or ceramic.

Fiber Reinforced Polymer Composites, or FRP Composites in short, are lightweight, strong materials used in the manufacturing of numerous products used in our daily life. FRP Composites, is a term used to describe a fiber reinforced composite material that uses fibers as the primary structural component and thermosetting resins such as epoxy, polyester, or vinyl ester as the matrix.
FRP main advantages are:

a) High tensile strength combined with its low weight. For example, a decent rule of thumb when comparing steel to CFRP composites is that a carbon fiber structure of equal strength will often weigh 1/5th that of steel
b) High stiffness
c) High durability and excellent fatigue properties

d) Good adaptation to loading conditions

The main disadvantages are:

a) Totally brittle failure. It has no plastic behavior, so it has not the ability to absorb energy
b) Anisotropic response and strength. There are many variables that could change its behavior and strength. The grade and quality of materials, the manufacturing process, fiber architecture, and the quality need to be taken into account.

There are mainly three kind of fibers, Carbon, Aramid and Glass fibers. Composite materials, reinforced with carbon fiber, are different than other FRP composites using traditional materials such as fiberglass or aramid fiber. The properties of CFRP composites which are advantageous include:

- Light Weight. A traditional fiberglass reinforced composite using continuous glass fiber will commonly have a larger density than a Carbon FRP composite, with the same fiber weight
- Higher strength and stiffness. Not only carbon fiber composites are lighter weight, but CFRP composites are much stronger and stiffer per unit of weight. This is true when comparing carbon fiber composites to glass fiber and aramid fibers, as shown in Figure 1.11.

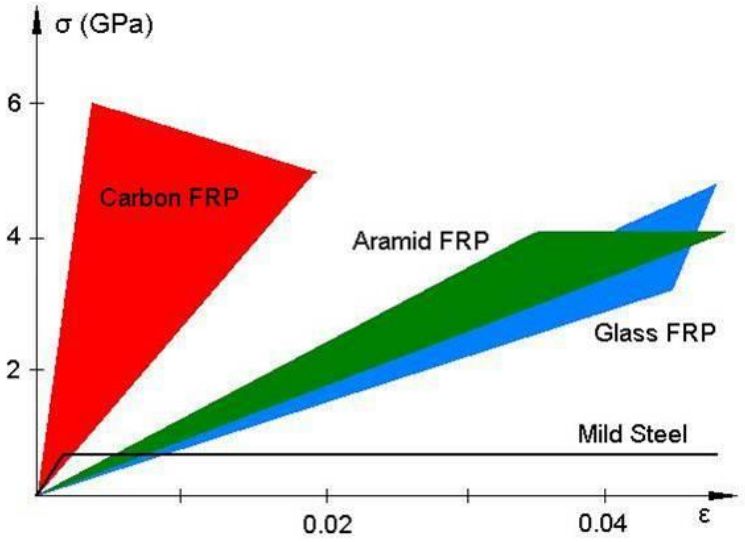

Figure 1.11: Comparison between Carbon, Aramid and Glass FRP

Disadvantages of Carbon FRP Composites:

- Cost. At the moment, CFRP composites are cost prohibitive in many instances. Depending on the current market conditions (supply and demand), the type of carbon fiber (aerospace vs commercial grade), and the fiber tow size, the price of carbon fiber can vary dramatically. Carbon fiber's price can be 5 to 25-times more expensive than fiberglass. This disparity is even greater when comparing steel to CFRP composites.
- Conductivity. This can be both an advantage, or a disadvantage depending on the application. Carbon fiber is extremely conductive, while glass fiber is insulative. Many applications use glass fiber, and cannot use carbon fiber or metal, strictly because of the conductivity

Although the cost of CFRP composites remains high, new technological advancements in manufacturing are in progress to allow more cost-effective products. Probably, in a short

time cost-effective carbon fiber is going to be used in a wide range of consumer, industrial, and automotive applications. The most common CFRP products are wraps, with thickness from 0.1-0.5mm, and plates with thickness from 1-5mm. (Figure 1.12)

a) b)

Figure 1.12: Carbon FRP a) wraps and b) plates

Among the most commonly used materials for fibers (glass, carbon, aramid), the bigger part of the literature highlights that carbon fibers are the best solution for structural steel strengthening as it is for concrete structure, because of its high strength and stiffness, excellent fatigue properties and large durability. For the scope of this thesis, CFRP plates are preferred instead of wraps or strips for angles strengthening because it is easier to apply them on angles.

1.3.2 Application procedure

In order to ensure the best possible adhesion of the composite materials with the steel members and to prevent oxidation of steel surface, it is necessary the appropriate preparation of both surfaces. The CFRP plate need to be cleaned with acetone to remove any dust on it. Regarding the steel surface, it is usually painted or galvanized and maybe rusted, so sandblasting is the most common solution to remove all of it and then optionally a primer liner can be applied to protect steel, especially in case of using epoxy resin. It has to be noticed that sandblasting is not an easy procedure when applied onsite on existing steel structures. The thickness kai the uniformity of the resin layer is very crucial. It is recommended that the resin layer should be among 0.25-2mm thick. The basic layers and the procedure step by step are described in Figure 1.13. This procedure ensures that a rigid adhesion is made between the two materials and so no bonding failure occurs

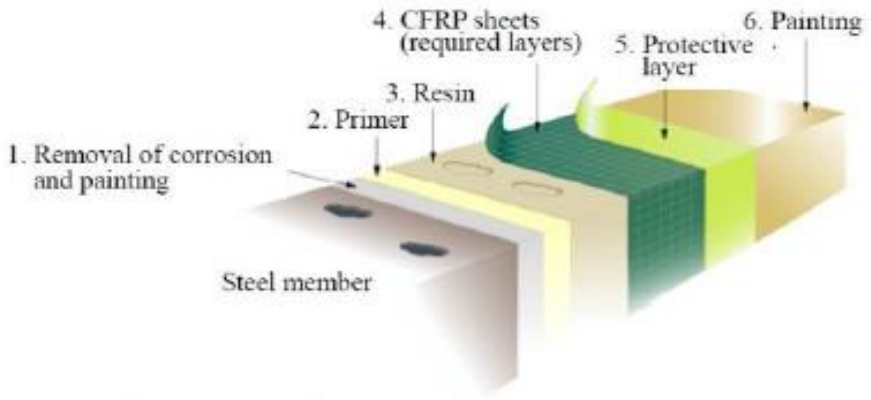

Figure 1.13: Application of the CFRP plate on a steel member

2 Experimental tests on steel plates with CFRP strengthening

2.1 Introduction

For the best possible design of a steel structure strengthened with CFRP plates a crucial factor is the estimation of the steel section's response after application of the CFRP plate. Because both literature and experimental test on steel sections combined with CFRP plates are limited, it is needed to be executed several experimental tests on steel sections strengthened with CFRP plates.

In this chapter the results of the experimental tests on steel plates strengthened with Carbon Fiber Reinforced Polymer (CFRP) plates are presented. These tests were executed in the Institute of Steel Structures at NTUA. Three composite (steel-CFRP) specimens were fabricated and were tested on three different ways. The first test was a tensile test while the other two tests were four-point bending tests. The difference between the second and the third test is that in this bending test the CFRP plate is on the tension side of the specimen while on the third test it is on the compression side.

Subsequently, the fabrication of the specimens is described analytically as well as the material properties and the testing set-up. Then, the experimental results are presented and are compared with the results occurred through analytical analyses and numerical analyses that were implemented with the ABACUS finite elements software. The main information about these tests is described in "Vlachaki – Karagiannopoulou S. G. (2018). Behavior of reinforced polymers with experimental and analytical methods. Diploma Thesis, Institute of Steel Structures, NTUA" [1].

2.2 Description of specimens

2.2.1 General

The steel specimens with CFRP strengthening were constructed at Brandenburg University of Technology (B-TU) in Germany. All specimens had the same dimensions and were made by the same material. Each one was consisted by two parts, a 3mm thick steel plate with dimensions 80x250mm and a 1.2mm thick CFRP plate with the same dimensions (80x250mm). The two parts were bonded with a structural adhesive along their whole surface, with approximately a thickness of 1.3, 1.1 and 1.1 mm for the specimens 1,2 and 3 respectively. Two aluminum tabs with dimensions 84x100x3mm were also used at the specimens ends on the side of the CFRP plate, in order to protect fibers and avoid a local failure or fibers' break at the sections that are attached in the machine's grips in tensile test or at the points of load application in bending tests. The side and plan view of the specimen is shown in Figure 2.1. In Figure 2.2 specimens are shown before testing.

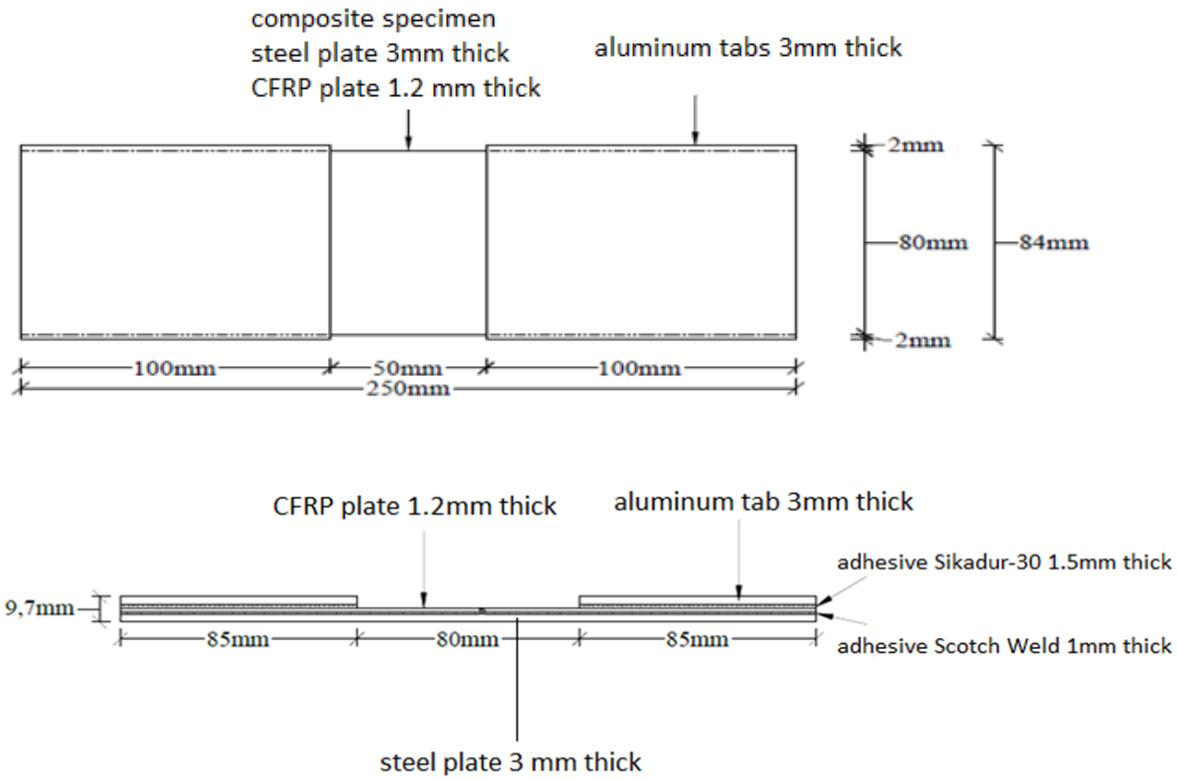

Figure 2.1: Plan and side view of the specimen

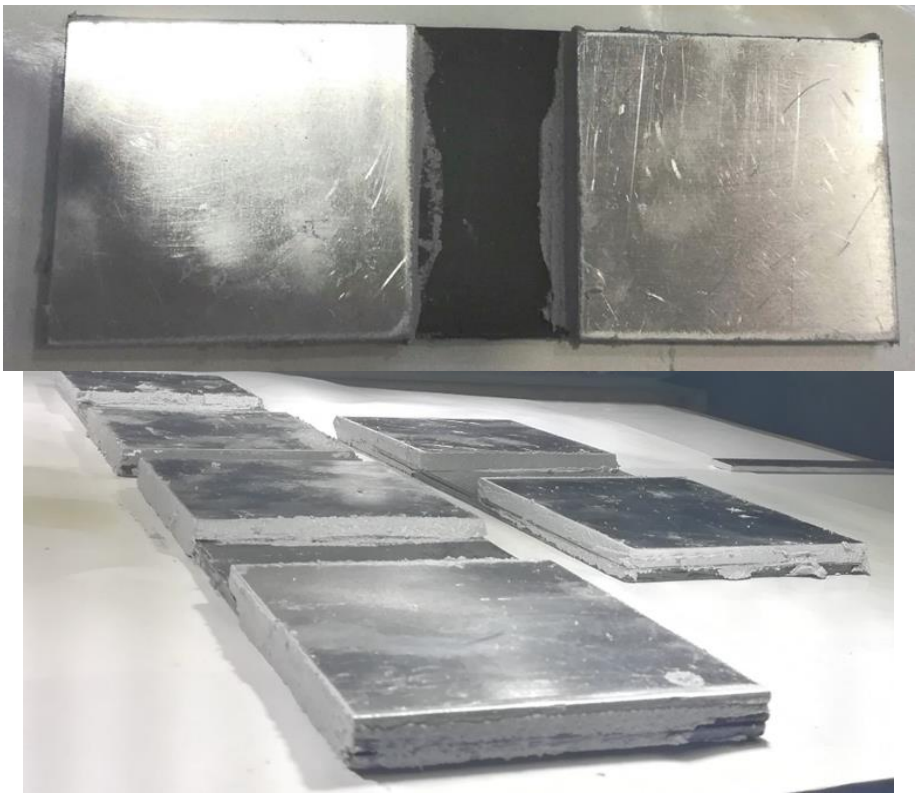

Figure 2.2: Pictures of the specimens before testing

2.2.2 Materials

Steel

Steel's exact material properties are unknown, so they must be exacted through experimental tests on steel specimens. For this purpose, two tensile tests were executed on steel specimens made from the same material. The test procedure is analytically described in [1]. According to test's results, Figure 2.3 shows steel's stress-strain curve. The characteristic values of steel's properties are shown in Table 2.1.

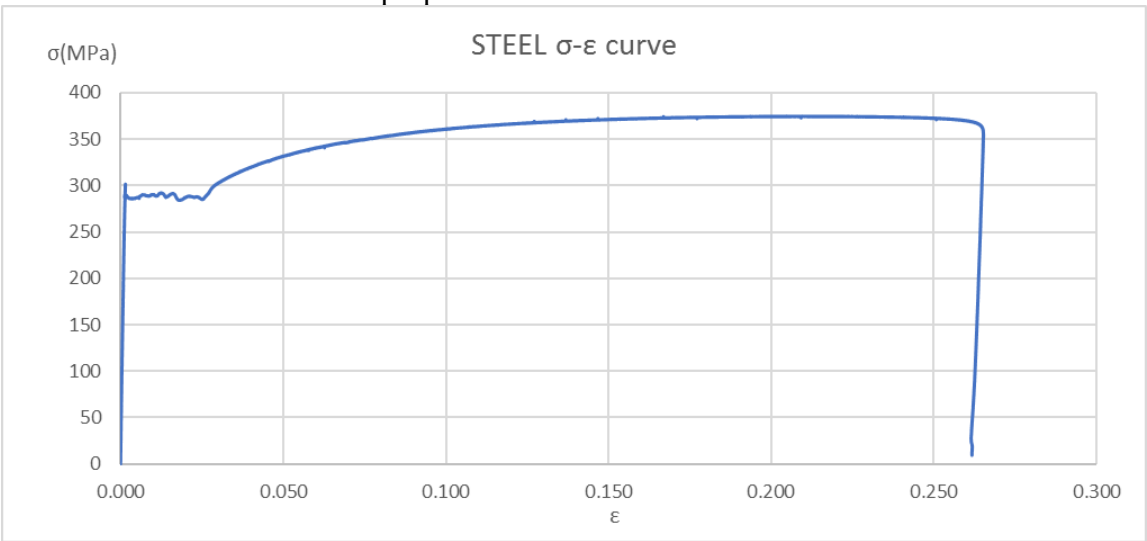

Figure 2.3: Steel stress-strain experimental curve

Table 2.1: Characteristic values of steel's properties

E (MPa)	Yield stress σ_y(MPa)	Yield strain ε_y(%)	Hardening stress σ_R (MPa)	Hardening strain ε_R(%)	Ultimate stress σ_{max} (MPa)	Ultimate strain ε_{max} (%)
210000	287.5	0.1364	291	2.886	375	39.818

Carbon Fiber Reinforced Polymer (CFRP)

The CFRP plates used in the tests are made by MC Brauchemie and are typically concerned as "low strength" plates. Their type is 160/2400 which means that their theoretical Young's Modulus is 160 GPa and ultimate strength is 2400 Mpa. Accordingly to their producer, CFRP plates were made using unidirectional fibers, with 0^0 angle to the longitudinal axe of plate. No other material properties were known due to terms of confidentiality. For this reason, as well as to estimate the actual mechanical properties of this material seven tensile tests were executed on CFRP specimens made by the same material. Two standards were taken account for the estimation of Young's Modulus E, DIN EN ISO 527-4 [2] and ASTM D638 -03 [3], D3039 [4]. There were also executed numerical analyses on finite elements models using ABACUS software package to validate the results. The testing procedure and the results of the experimental tests and numerical analyses are included in [1]. As concluded, CFRP plates have an elastic behavior. Their failure is brittle and no plastic strains occur. Based on these tests the average values for the material' characteristics are given in Table 2.2.

Table 2.2: Average values of CFRP's properties

E (MPa)	Max stress σ_{max} (MPa)	Max strain ε (%)
141000	2734	1.91

Adhesive

The adhesive that was used to bond steel and CFRP plate is the structural epoxy resin Scotch WeldTM DP 490 (Figure 2.4a), which is characterized by its simple and easy application, and accordingly to its producer it is appropriate for using in steel sections. Its ultimate shear stress τ_k and normal stress σ_k are estimated based on [5] and are shown in Table 2.3.

In addition, for the bonding of aluminum tabs to CFRP plates a different epoxy adhesive was used, Sikadur 30, with a shear strength of 20 Mpa, accordingly to its producer. (Figure 2.4b).

Table 2.3: Adhesive's properties

¤	E_k (MPa)¤	σ_k (MPa)¤	G_k (MPa)¤	τ_k (MPa)¤
μ¤	3063¤	3,76¤	308,9¤	3,44¤
σ¤	0,218¤	0,053¤	0,069¤	0,032¤

a) b)

Figure 2.4: a) Epoxy resin Scotch Weld DP490 b) epoxy resin Sikadur 30

2.2.3 Preparation of specimens

As it was mentioned before, the specimens were fabricated at Brandenburg University of Technology (B-TU). A special procedure was followed. Firstly, a special treatment using a hard brush was implemented to the steel surface, to increase surface's roughness in order to have better application of the adhesive. Then the surfaces of both steel and CFRP plates were cleaned with acetone. The adhesive was added using a special equipment (Figure 2.6). The adhesive has to be applied uniformly, with an equal thickness of approximately 0.2mm all over the surface. For this purpose, small beads with diameter 0.105-0.20 mm made from glass were placed between the two surfaces as seen in Figure 2.6. The two bonded plates remained under constant pressure for seven days until the adhesive reached its total strength. However, after this procedure the adhesive's thickness was measured and was found to be 1.3, 1.1 and 1.1 mm for specimens 1,2, and 3 respectively.

Figure 2.5: Surface's preparation and cleaning

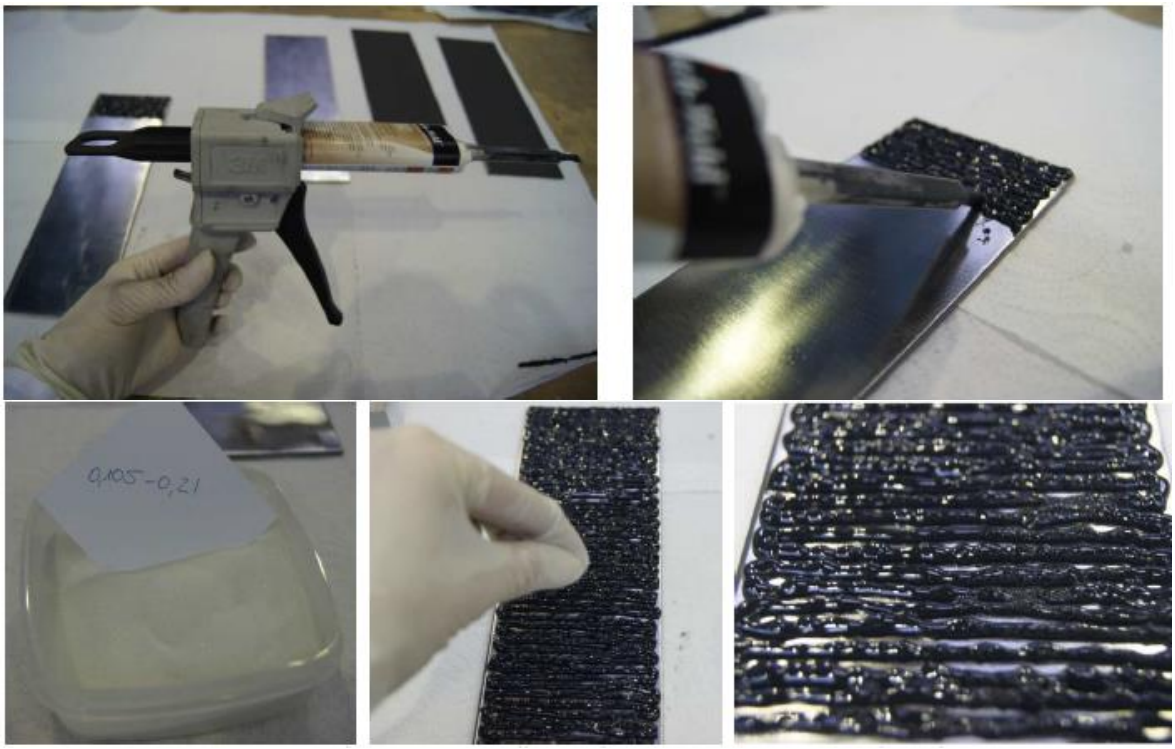

Figure 2.6: Application of the adhesive using special equipment

Afterwards, two aluminum tabs were also bonded on the CFRP side to protect fibers from local failure and break in certain parts of the CFRP plate where the load is locally applied. A different adhesive was used to bond the aluminum plates to CFRP plate (Sikadur 30). After that the three specimens remained seven more days under some heating lamps at a constant temperature of 33-36^0 C, so that adhesive reaches its maximum strength. The three specimens are shown in Figure 2.7.

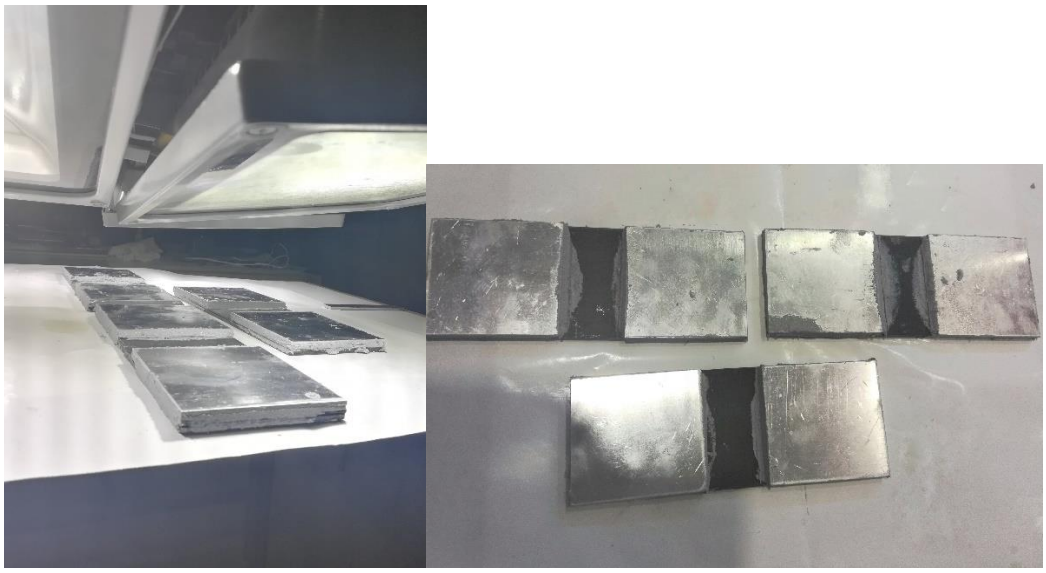

Figure 2.7: Steel specimens with CFRP strengthening

2.2.4 Numerical modeling

In order to validate the results from the tests, several numerical analyses have to be executed. The three tests are simulated numerically using finite element modelling in ABAQUS-CAE software package. For each test a separate model is used.

Model geometry

Each component of the specimen is simulated as separate part with its real dimensions (250x80mm) and thickness, 3mm for steel plate, 1.2mm for CFRP plate and 1.3/1.1 mm for the resin. The parts are modelled as by means of 3D deformable solid elements. The aluminum plates are not modelled since they don't affect significantly the specimen's response. The interaction between the surfaces of the parts is assumed as tie constrained, which means that no slip is allowed between the plates. It is an assumption close to reality since there was no such an observation in the executed tests.

Materials

The material properties that are assigned in the models are based on the executed tests and on the values that are referenced in Paragraph 2.2.2. More specifically, regarding the steel, it is considered elastoplastic response with hardening. The Young's modulus is $E = 210000\ Mpa$, and the plastic stress-strain curve is imported in Excel table format that occurred from the executed tensile tests. Consequently, this is the actual stress-strain curve of steel material.

Regarding the CFRP material, an anisotropic elastic material is considered, with the basic values that occur through the experimental tests and are referred in Paragraph 2.2.2. regarding the Young's modulus, it is estimated on a repeated procedure through the numerical analyses and the tensile test and is used for the 4-point bending analyses

Support conditions

Support conditions were applied based on the real testing support conditions, which means that rolls were assigned at the nodes that cylindrical supports existed. The load introduction is made through displacement control of the nodes.

Analyses

Two main numerical analyses were executed. Firstly, an analysis only with nonlinear material is executed followed by an analysis with both nonlinear material and geometry.

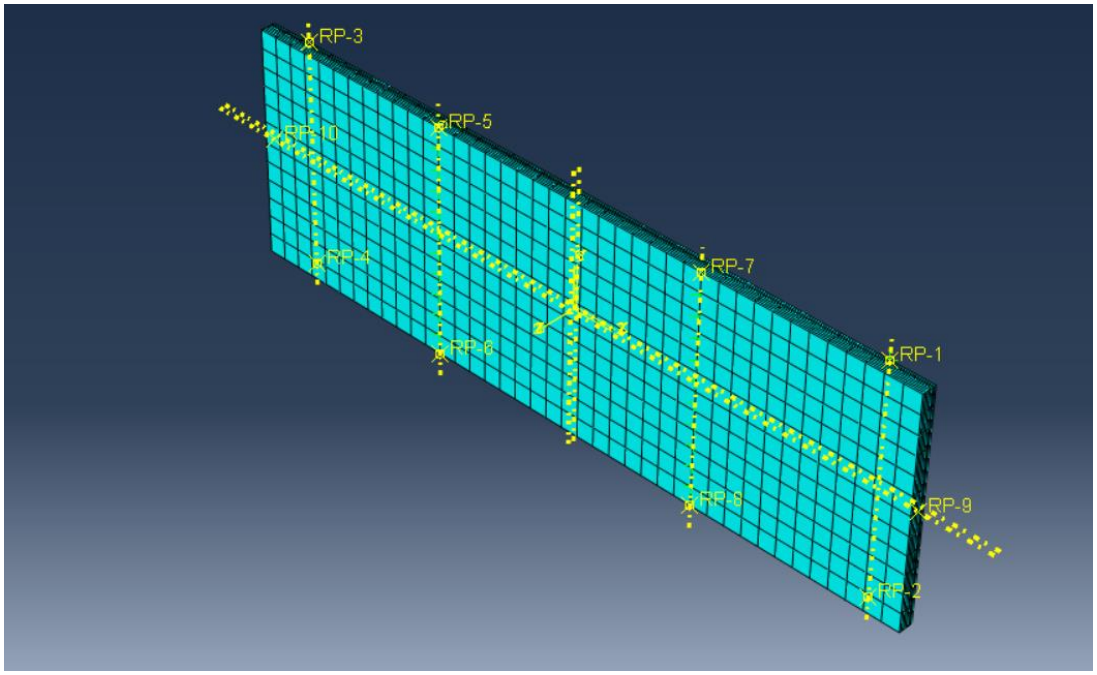

Figure 2.8:Numerical model on ABACUS

2.3 Tensile test

2.3.1 Testing set-up

It is a typical tensile set-up, where the load is imposed via displacement control with a speed of 0.2mm/min. Based on the characteristic strength of steel and CFRP plates and the equation 2.1 , it is concluded that failure in tension is not feasible due to machine's restrictions and total load capacity (maximum load 300 kN).

$$Pu = \sigma_{\max,\ frp} * A_{frp} + \sigma_{\max,\ steel} * A_{steel} = 360kN > 300kN \qquad \textbf{Eq. 2.1}$$

where,

$\sigma_{max,steel} = 387\ MPa$

$\sigma_{max,frp} = 2780\ MPa$

$A_{frp} = 96\ mm^2$

$A_{steel} = 240\ mm^2$

So, the tensile test was executed until the maximum load capacity of the machine (300 kN). As it was expected the specimen didn't reach failure, however this test is important in order to estimate the mechanical properties of the CFRP plate, especially the Young's Modulus, which is needed to be known in bending tests. Two stain gauges were assigned on both sides of the specimen (on steel and CFRP) to measure the materials' strain. The total tension load and the specimen's elongation was also measured during the test. The testing set-up and measurement equipment is shown in Figure 2.9: Testing set-upFigure 2.9 and Figure 2.10.

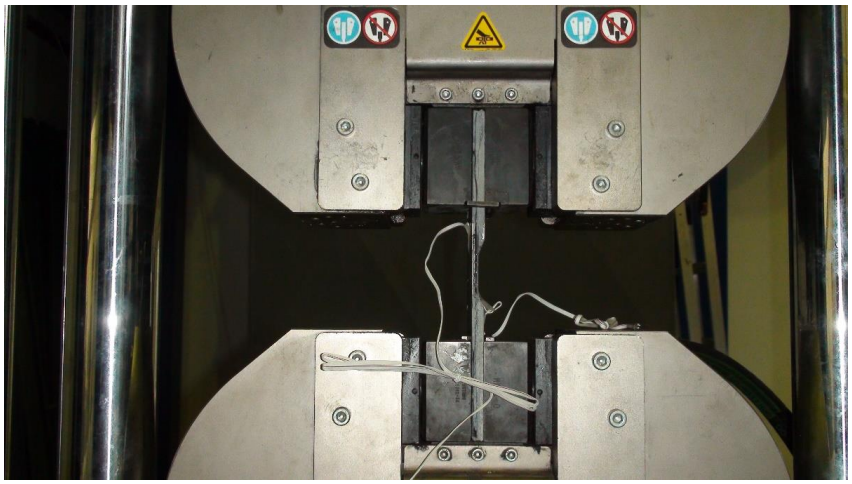

Figure 2.9: Testing set-up

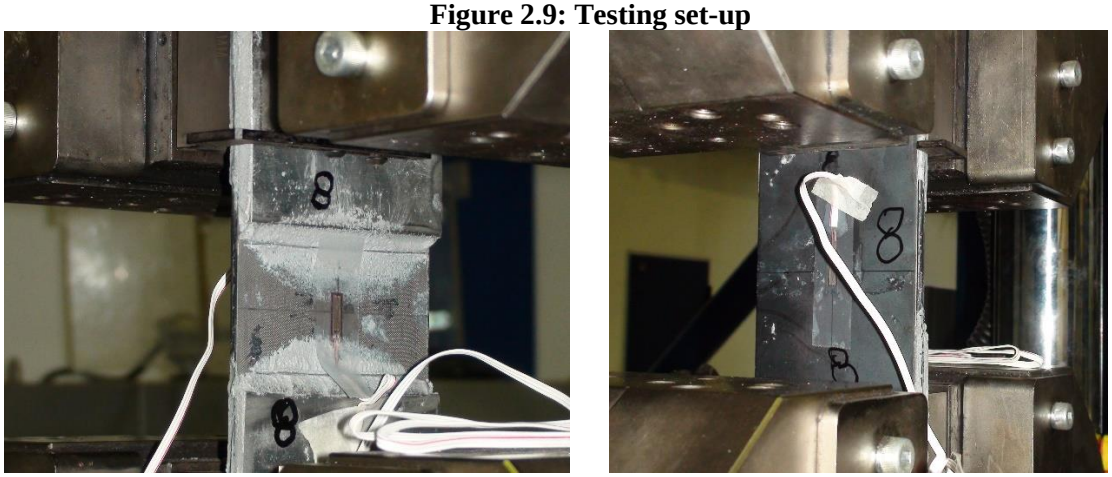

Figure 2.10: Instrumental measurement (strain gauges)

2.3.2 Test Results

As it was expected the specimen didn't reach to failure. However, after the end of the test it was observed that the specimen had a residual deflection as shown in Figure 2.11.

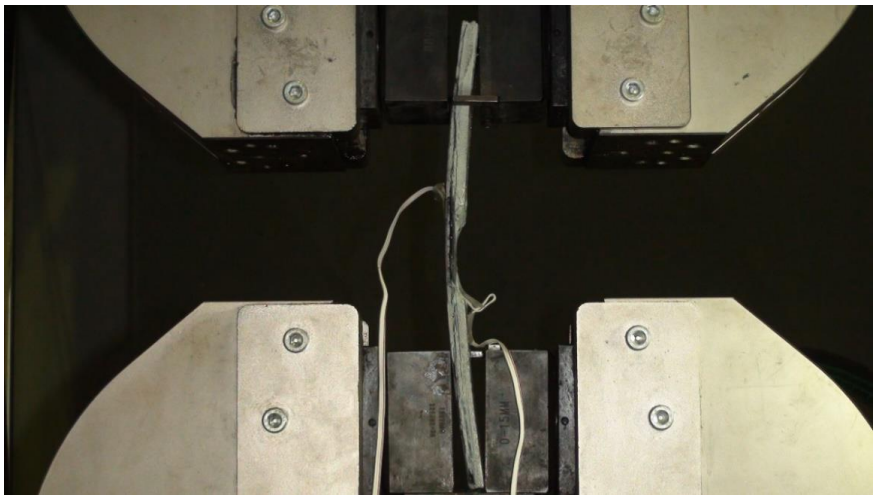

Figure 2.11: Permanent deflection of the specimen

The whole testing procedure as well the analytical and numerical analyses are analytically described in [1], where the following main results are mentioned. The experimental load-displacement curve is shown in Figure 2.12. Figure 2.13 shows the strain of each material separately during the tensile test. Although, the specimen elongation is common for both materials, it is noticed that strains are not the same. This is obviously observed because of the loading eccentricity that exists and makes the specimen to develop an internal resistant moment, which has as a result the different strains measured at each side of the specimen.

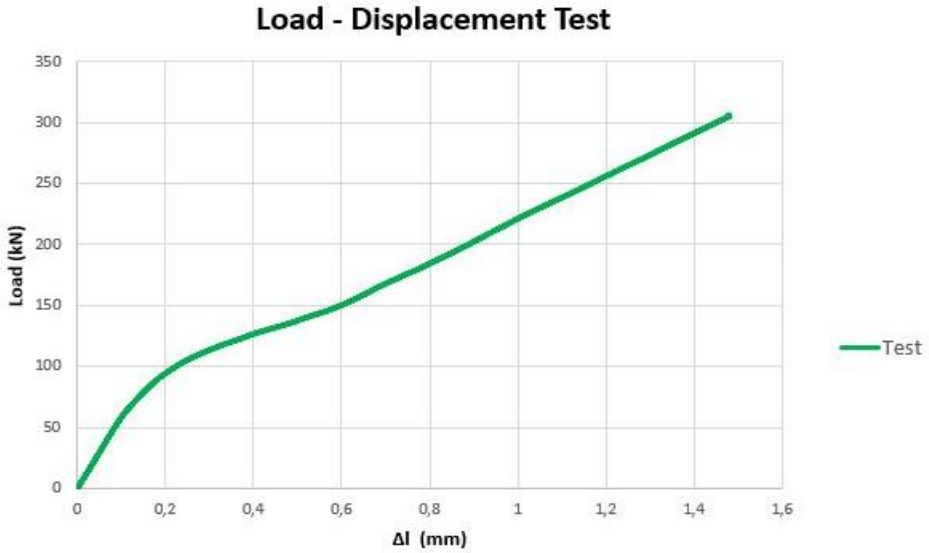

Figure 2.12: Experimental load-displacement curve

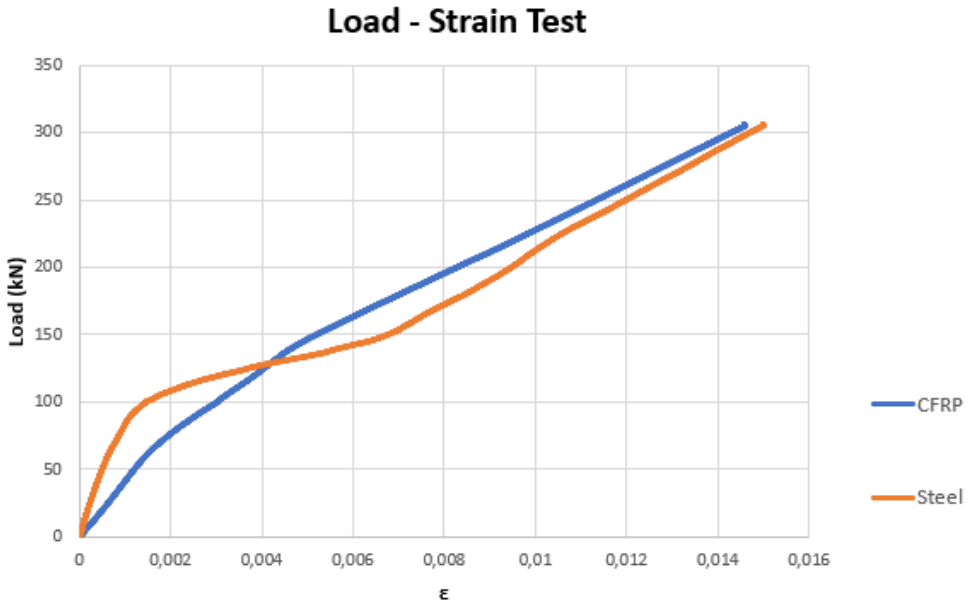

Figure 2.13: Experimental Load-strain diagram for the 1st specimen

Based on the geometry of the specimen (Figure 2.14) and the methodology described in [1], the permanent strain is calculated as equal to:

$$\varepsilon_{perm} = \frac{L_{arc,\,tot} - L_{linear}}{L_{linear}} = \frac{(127,67 + 127,53) - 251,75}{251,75} = 0,0137 \qquad \textbf{Eq. 2.2}$$

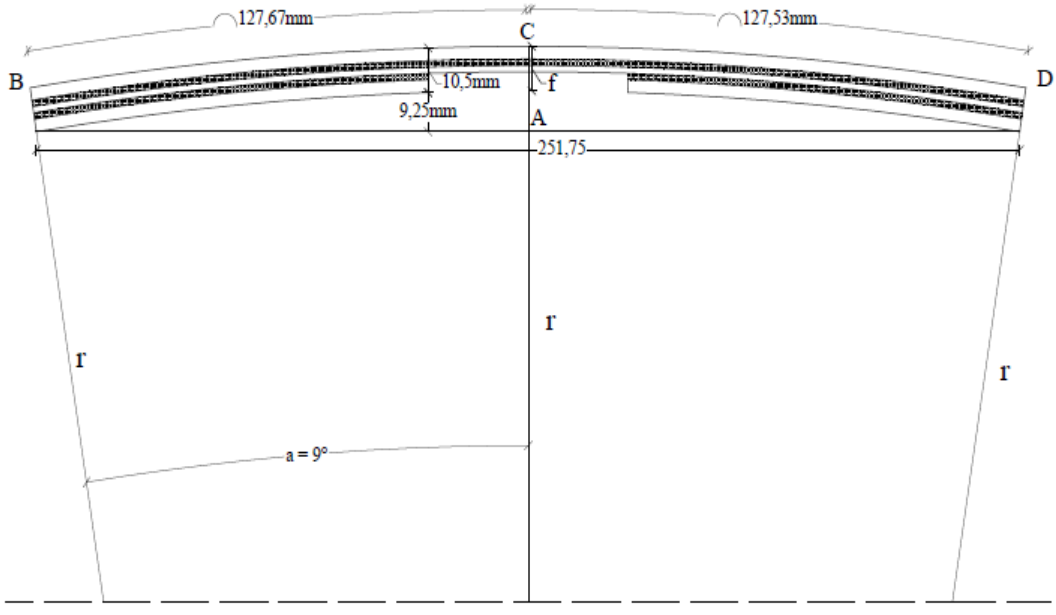

Figure 2.14: Geometry of the specimen after the test

2.3.3 Analytical and numerical results

Following the analytical methodology that is introduced in [1] and is shown in Figure 2.15 the total tensile load can be calculated analytically and can be compared with the experimental results. After an iteration procedure where the Young's modulus of CFRP

material increased incrementally, the final analytical load-displacement curve occurred. For a value of E_{FRP}=166000 Mpa the analytical and the experimental curves match perfectly as shown in Figure 2.16. For this reason and because the other two specimens were made from the same CFRP plate this Young's modulus value is used for the analyses at the 4point bending tests.

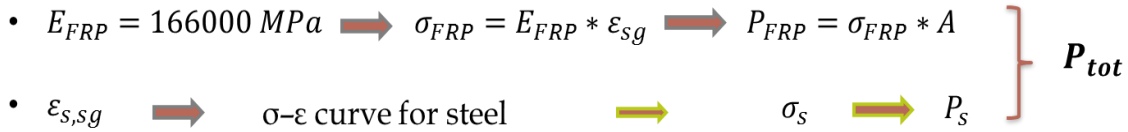

Figure 2.15: Analytical methodology for the calculation of the total load

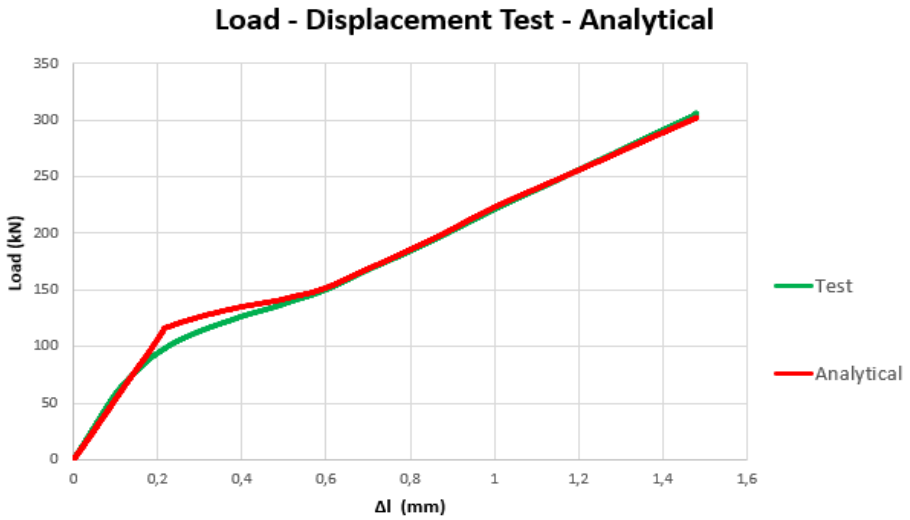

Figure 2.16: Comparison between analytical and experimental load-displacement curves

Finally, Figure 2.17 shows the comparison between the Moment-displacement curves that occurred through testing, analytical and numerical analysis. It is noticed that that there is a difference between the internal moments due to the eccentricity load introduction during testing, which can be estimated/

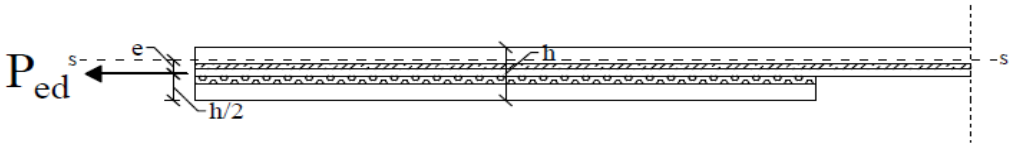

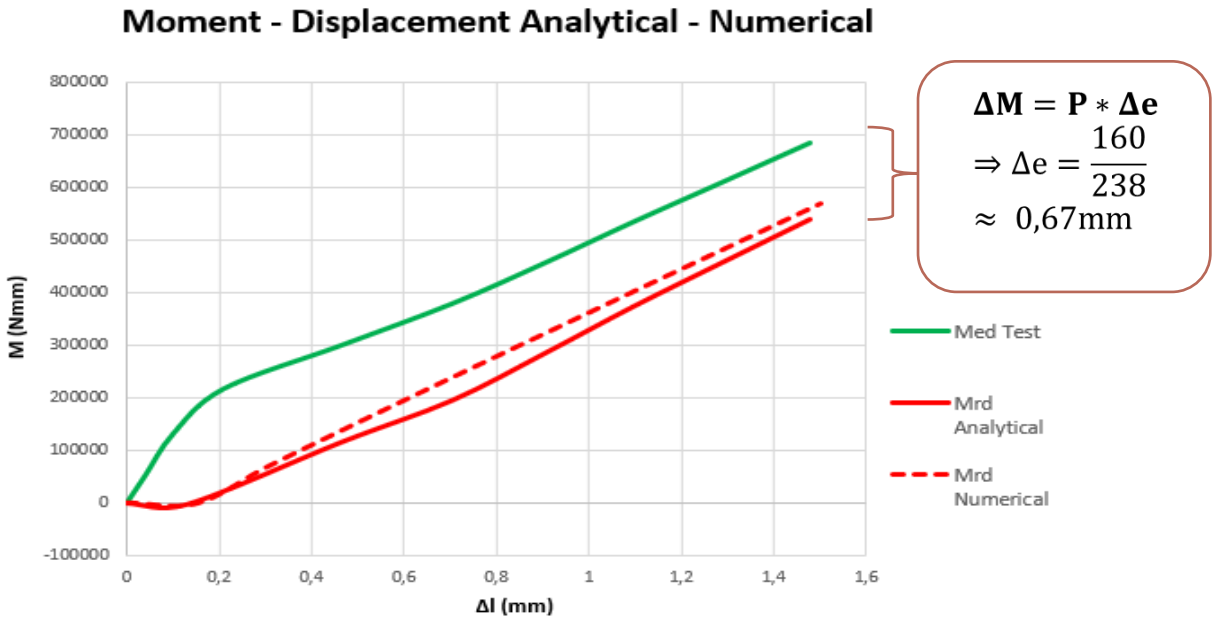

Figure 2.17: Comparison between experimental, analytical and numerical M-d curves

2.4 1st Four-point bending test (CFRP plate on the tension side)

2.4.1 Testing set-up

The set-up for the four-point bending test is shown in Figure 2.18. The CFRP plate is placed on the tension side of the specimen. The load was applied via displacement control with a speed of 0.420 mm/min. Figure 2.19 shows the specimen before and during testing. Two stain gauges were assigned on both sides of the specimen (on steel and CFRP) to measure the materials' strain. The total load and the specimen's deflection was also measured during the test.

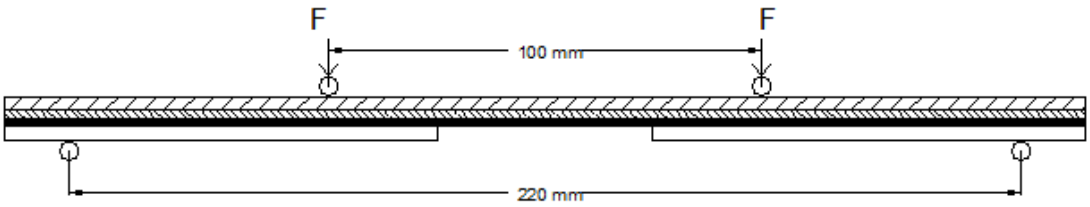

Figure 2.18: Testing set-up for the 2nd specimen

Figure 2.19: Specimen before and during testing (CFRP on the tension side)

2.4.2 Test results

The specimen exhibits an inelastic response with large plastic strains. This had as a result very big deflection at the end of the test, which finally lead the specimen to slide from its position and fail. Small slip was also indicated at certain times during the test. The force-displacement diagram of the test is shown in Figure 2.20. Using Eq. 2.3 for the calculation of bending moment, the M-d diagram is calculated (Figure 2.21). Figure 2.22 shows the stress-strain curves for the two materials, measured by the strain gauges. It must be noticed that steel's strain data were not recorded until the end of the test, because the strain gauge at the compression side of the specimen was disconnected due to large strain.

$$M\exp = \frac{F\exp}{2} \times l/2 \quad \textbf{(kNmm)} \qquad \text{Eq. 2.3}$$

where,
Fexp is the total load measured by the machine
l is the distance between supports and is equal to 220 mm

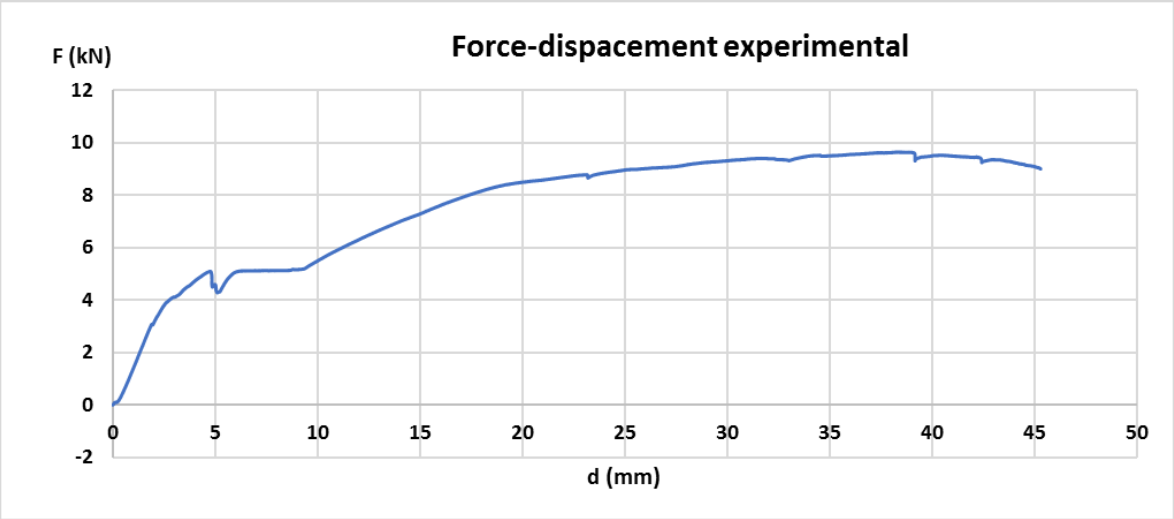

Figure 2.20: Experimental F-d curve

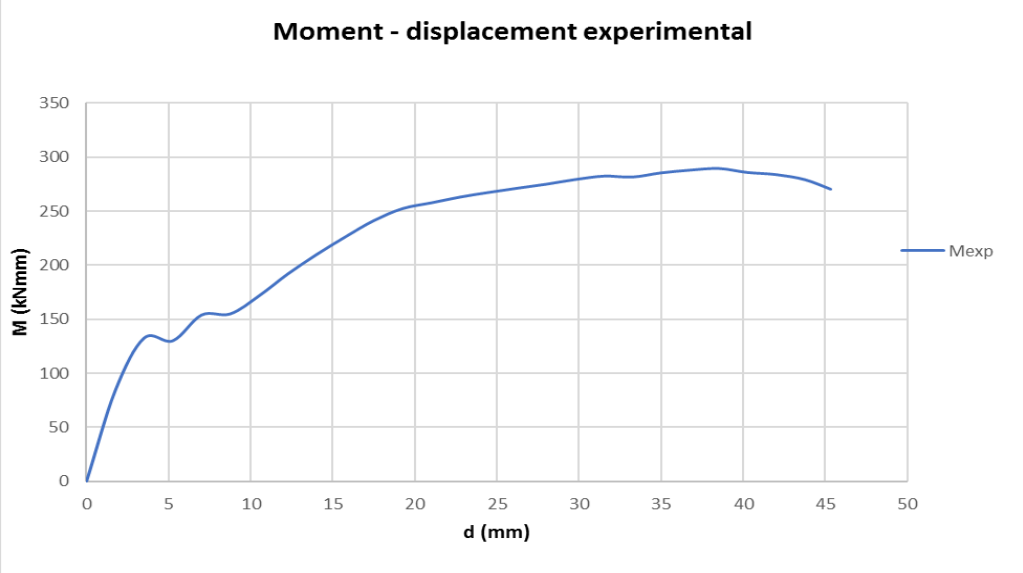

Figure 2.21: Experimental M-d curve

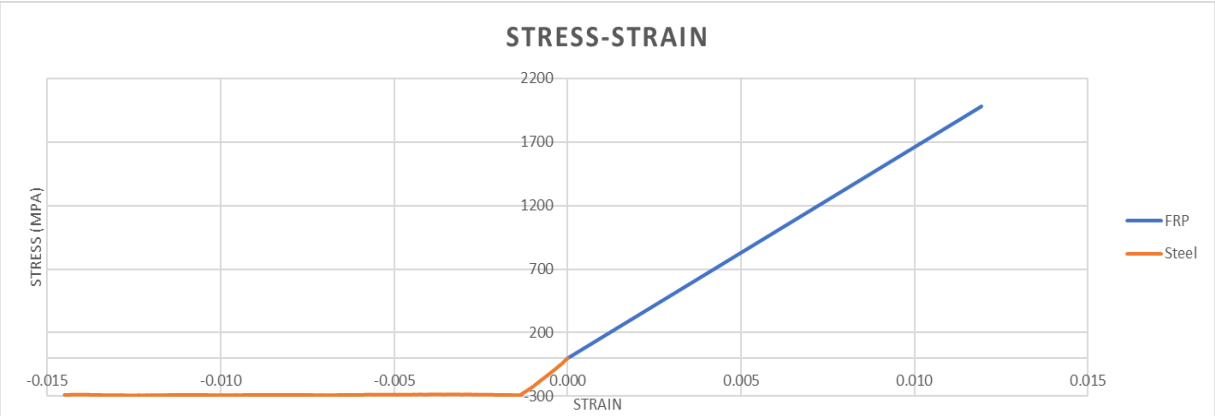

Figure 2.22: Experimental σ-ε curve for each material

It is noticed that steel yields and is in the plastic range of its curve, while CFRP exhibits a totally elastic behaviour until the end.

2.4.3 Analytical calculations

Using the experimental strain data and some theoretical equation, composite section's moment resistance is estimated and is compared with the experimental values. Two different methodologies are used.

Analytical Method 1

In this calculation method Bernoulli-Euler beam theory is used and so the basic assumtion is the linear distribution of strains along the height of the composite section. The centroid z_c of the composite section is calculated from the top compression side using**Error! Reference source not found.Error! Reference source not found.** Error! Reference source not found.

where,

$z_s = 1.5\ mm$

$z_{res} = 3.55\ mm$

$z_{cfrp} = 4.7\ mm$

$A_s = 80x3 = 240\ mm^2$

$A_{res} = 80x1.1 = 88\ mm^2$

$A_{cfrp} = 80x1.2 = 96\ mm^2$

$n_{res} = E_s / E_{res} = 210000/3063 = .68.6$

$n_{cfrp} = E_s / E_{cfrp} = 210000/166000 = .1.265$

Subsequently, the section's moment resistance is calculated as following:

The steel section is divided in 10 smaller strips, with a height *dz= 3/10=0.3mm*. For every time step, starting from the strain recorded data for the two materials, and assuming a linear strain distribution over section's height, section's neutral axis is estimated using Eq. 2.5. Strains at each height are calculated using Eq. 2.6. For CFRP plate strain is calculated at its centroid z_{cfrp} .

$$z_{na} = \varepsilon_{so} \times \frac{h_{tot}}{\varepsilon_{so} + \varepsilon_{cfrp}} \qquad \text{Eq. 2.5}$$

$$\varepsilon_i = \varepsilon_{cfrp} + \frac{\varepsilon_{so} - \varepsilon_{cfrp}}{h_{tot}} \times z_i \qquad \text{Eq. 2.6}$$

where $z_i = (i) * \frac{dz_i}{2}$

$h_{tot} = 5.3mm$

Then, material σ-ε real curve is used to compute stresses σ_i. Then using Eq. 2.7, 2.8, 2.9 the acting internal axial forces *Fi* and finally the section's resistance moment M_R is calculated.

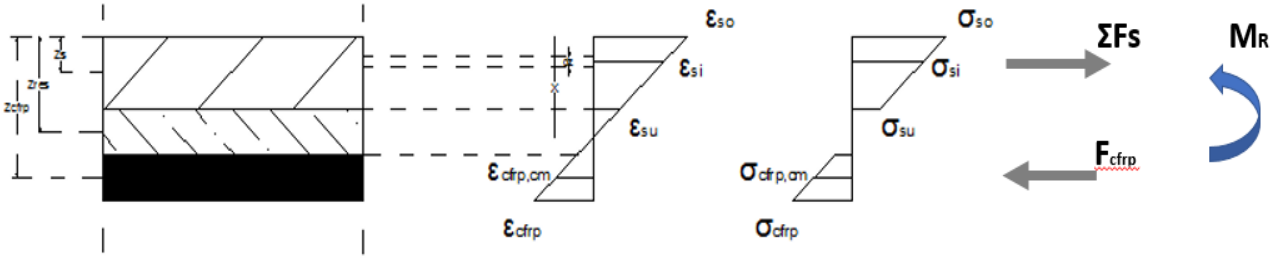

Figure 2.23: Section's resistance moment calculation (method 1)

$$F_{si} = \sigma_{si} \times dA_i \qquad \text{Eq. 2.7}$$

$$M_i = F_i \times (z_i - z_c) \qquad \text{Eq. 2.8}$$

$$M_R = \Sigma M_s + M_{CFRP} \qquad \text{Eq. 2.9}$$

As it is noticed in Figure 2.23 resin is ignored and is not taken account in this calculation. Regarding this methodology, there is a main disadvantage that no experimental data are available for the steel's strain until the end of the test, so it calculates M_R only up to a certain point.

Analytical Method 2

In this analytical method computed process is inverted. Starting from CFRP stain the internal axial CFRP force, F_{cfrp} , is calculated as following:

$$\sigma_{cfrp} = E_{cfrp} \times \varepsilon_{cfrp} \qquad \text{Eq. 2.10}$$

$$F_{CFRP} = \sigma_{cfrp} \times A_{CFRP} \qquad \text{Eq. 2.11}$$

Then using the equilibrium rule for the internal forces, F_s is calculated. Two basic assumptions are made so that calculations can be easy. Firstly, nolinear strain distribution is taken account. For both materials, stresses are considered constant over the section's height and so a different plastic neutral axe, z_{pna} ,is estimated. Secondly, as long as strain data for steel are available actual steel stress is used, afterwards it is considered that hardening stress occurs so a linear increasement in steel's stress is estimated until it reaches its ultimate stress at the end of the test. For CFRP material stress at its centroid is used, with the consideration that centroid's strain is approximately half of the measured

strain. More specifically, it is considered a linear strain distribution as if section's neutral axis was in the height of resin.

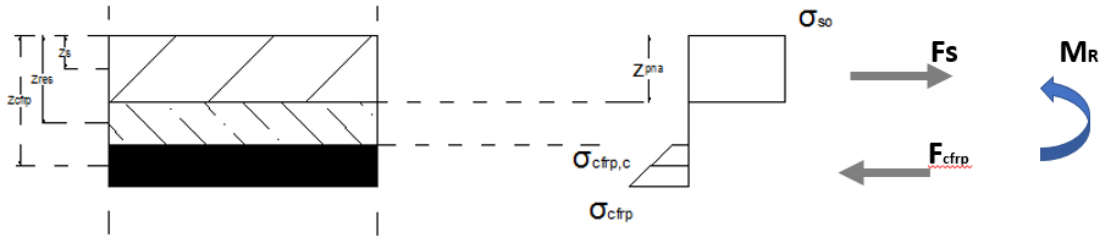

Figure 2.24: Section's resistance moment calculation (method 2)

$$F_s = F_{CFRP} \qquad \text{Eq. 2.12}$$

$$z_{pna} = \frac{Fs}{b \times \sigma_s}, \text{ where } b = 80 \text{ mm} \qquad \text{Eq. 2.13}$$

$$M_R = F_{CFRP} \times (z_{cfrp} - \frac{z_{rna}}{2}) \qquad \text{Eq. 2.14}$$

Comparing Experimental-Analytical results

A comparison between experimental results and analytical calculation of section's resistance moment (with both methods) is shown in Figure 2.25. The slip that was observed during testing is noticed in the experimental M-d curve.

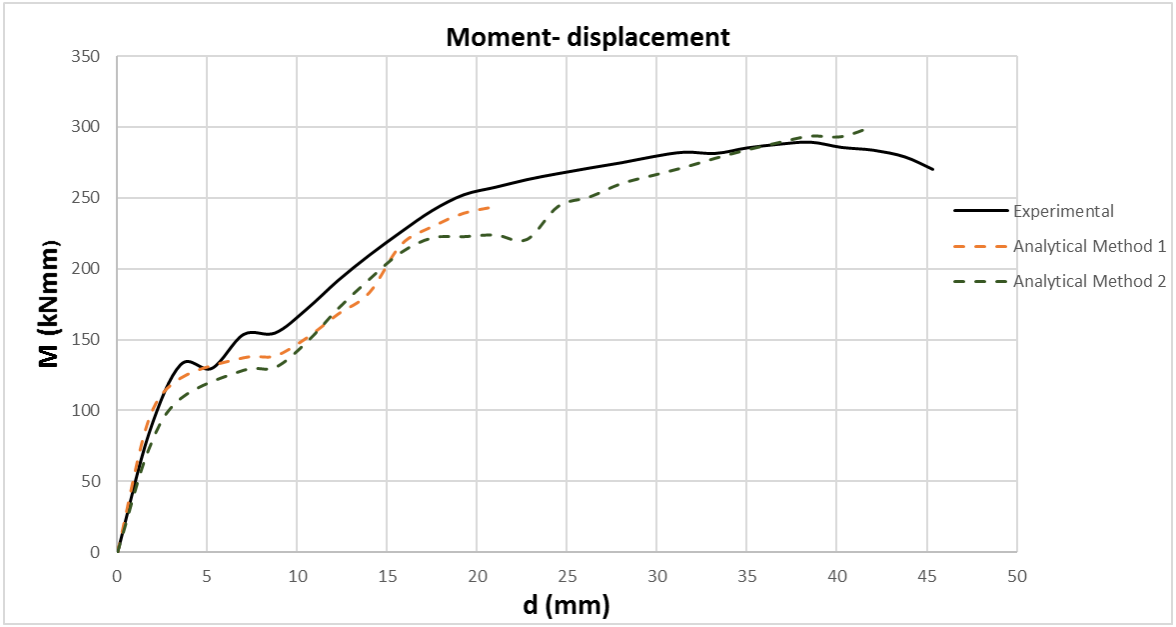

Figure 2.25: Diagram M-d

As it is seen values calculated with method 1 match with experimental results. There are some deviations, but this can be explained because a lot of assumptions have been considered and also the resin is ignored. Regarding method 2 it seems that results fit well with calculations only at large strains. This can be explained since assumptions made at this method are realistic only after steel yields, which means at plastic steel strain. In the part that strain data stop obviously a larger deviation is noticed. However, it is significant that despite missing data the curve reaches approximately at the same ultimate resistance moment as the test.

So, based on the above a new curve can be drawn based on both methods. From the beginning until the region that strain data stop values calculated with method 1 are used, and after that point values are estimated based on method 2. The new curve is shown in Figure 2.26.

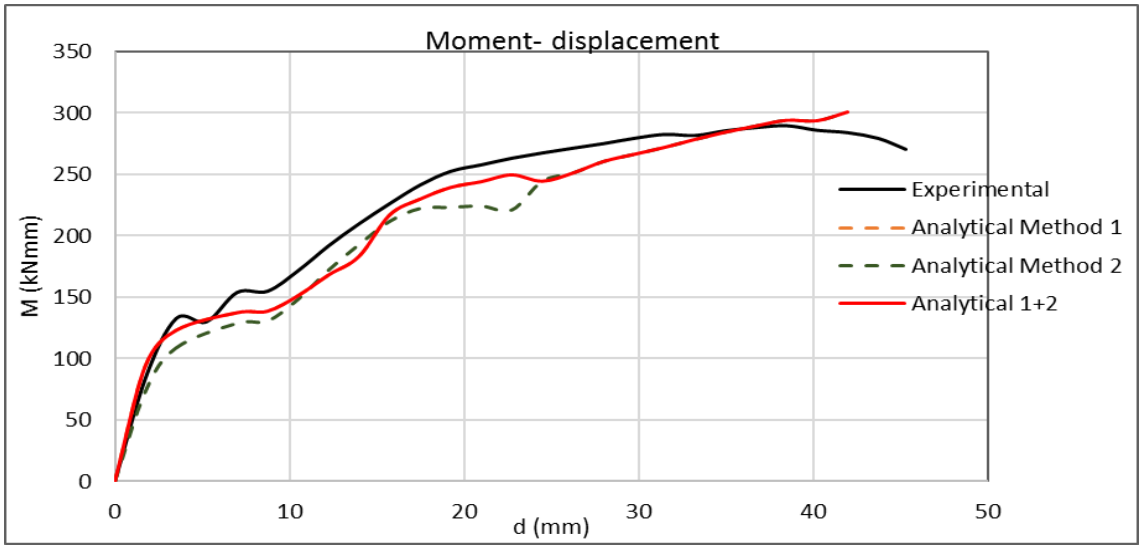

Figure 2.26: Diagram M-d based on both methods 1 and 2

2.4.4 Numerical results

In this paragraph the results from the numerical analyses are presented. As mentioned in Paragraph 2.2.4 two main analyses are executed, both regarding non linear material but only the second takes account nonlinear geometry. Figure 2.27,Figure 2.28 and Figure 2.29 show the deformation and the strain distribution on steel and CFRP plate.

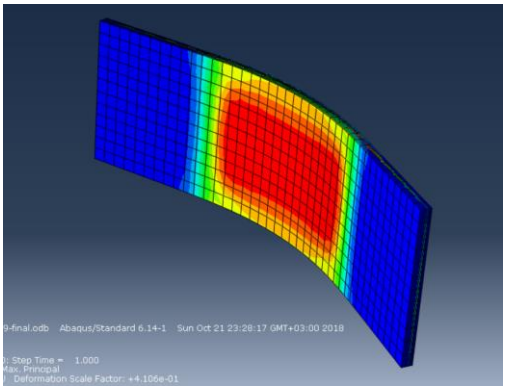

Figure 2.27: Deformed shape

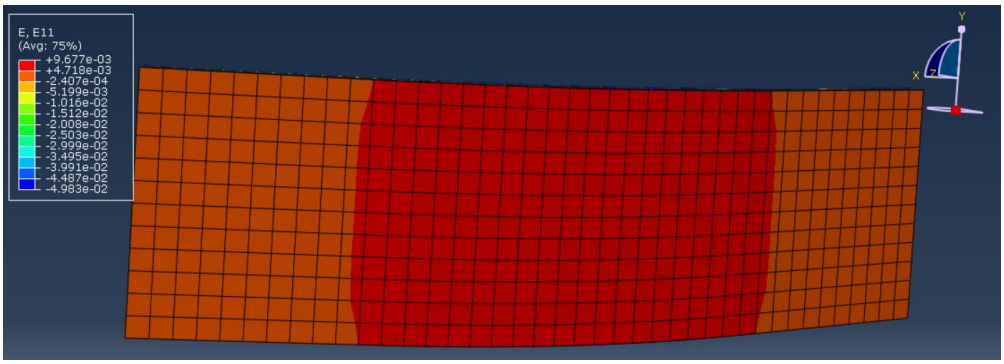

Figure 2.28: Strain distribution on CFRP

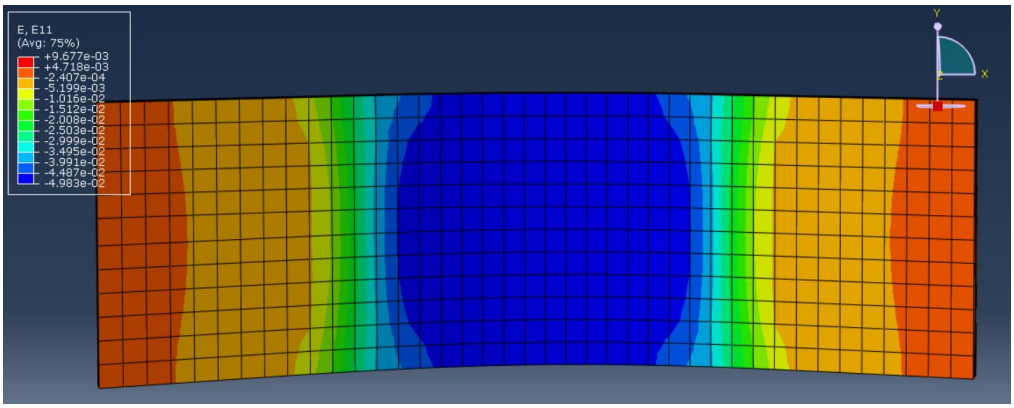

Figure 2.29: Strain distribution on Steel

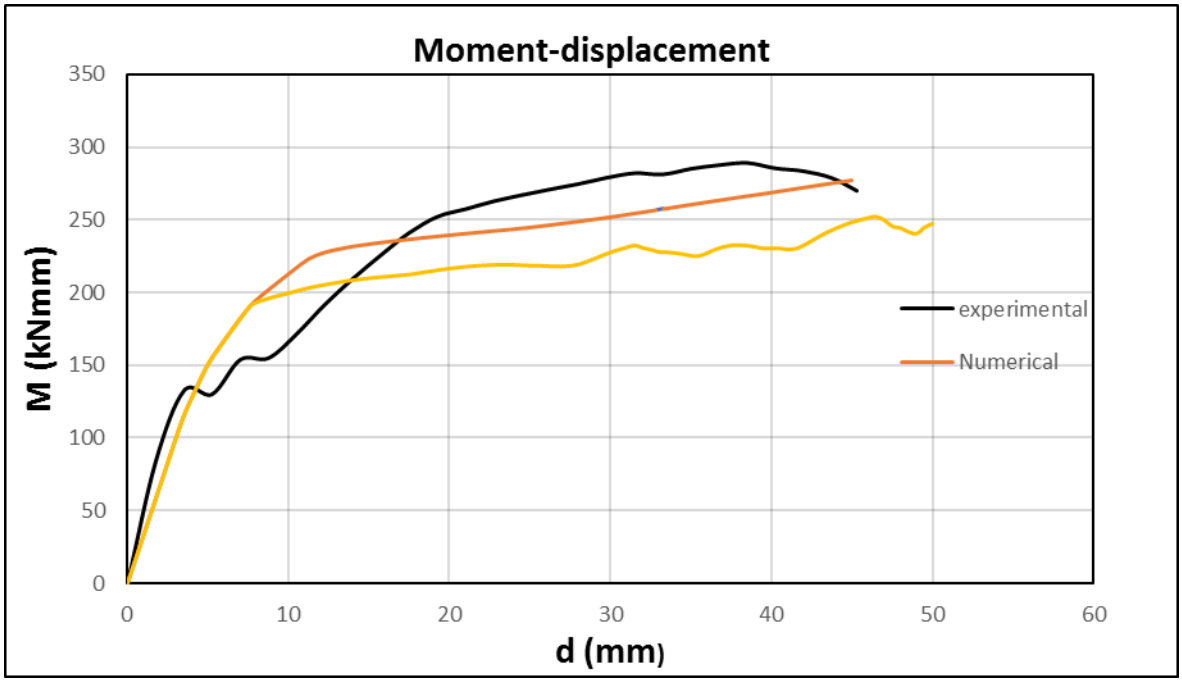

Figure 2.30: Numerical M-d curves

Figure 2.30 shows the moment-displacement curve that occurred by the numerical analyses. As it seen there is a good match at the elastic part of the curve. As it was mentioned before, a small slip was observed during the test. This is noticed in the experimental M-d curve and probably causes some deviation between the experimental and the numerical curves. A new corrected M-d curve (Figure 2.31) is calculated after removing the observed slip, to make a better comparison between the curves.

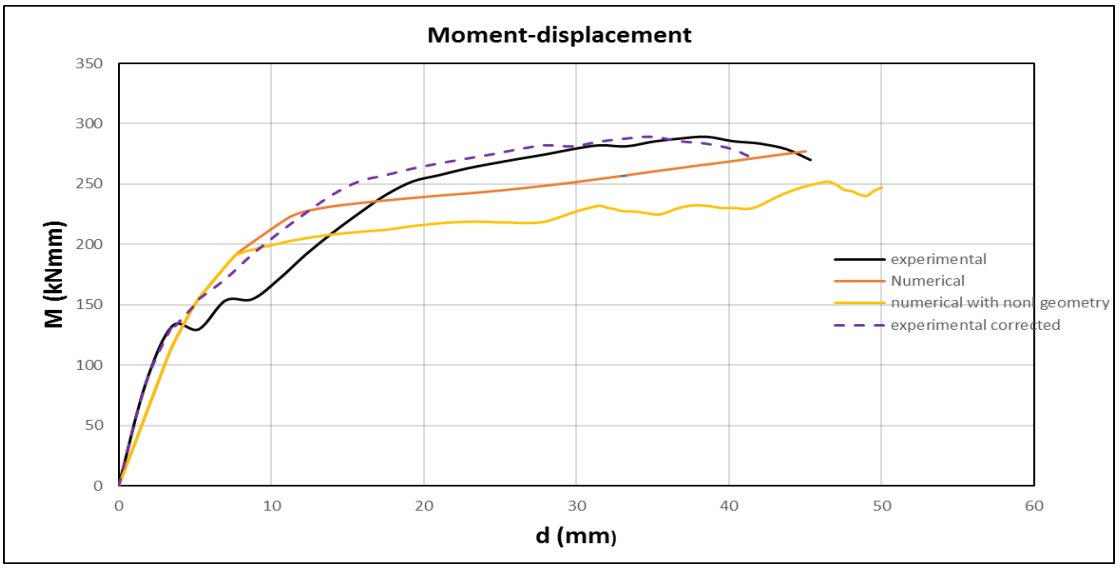

Figure 2.31: Corrected experimental M-d curve

Figure 2.32, Figure 2.33 and Figure 2.34 show the numerical stress-strain and stress displacement curves compared with the experimental results. It is noticed that the numerical CFRP σ-d curve differs significantly. The CFRP material at the numerical model does not reach the maximum stress that was measured in test.

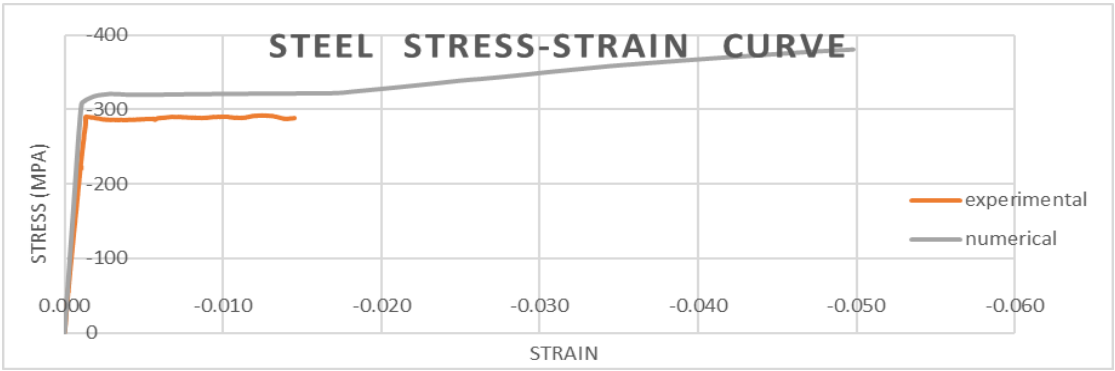

Figure 2.32: Numerical Steel σ-ε curve

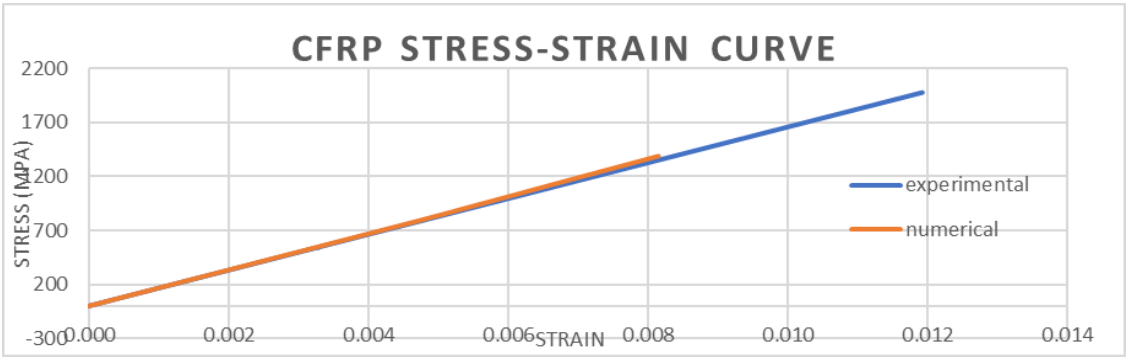

Figure 2.33: Numerical CFRP σ-ε curve

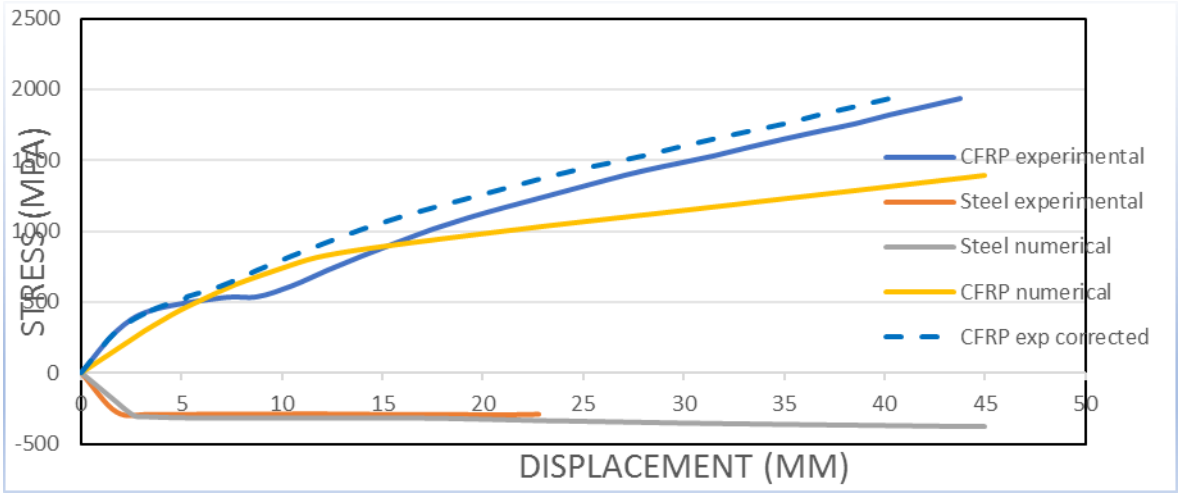

Figure 2.34: Numerical stress-displacement curves

Regarding the deviation on the CFRP stress between test results and numerical model, a possible explanation must be investigated in the resin's response. Since it is the only material that there were no testing data, the basic mechanic properties are estimated using literature or other sources. For this reason, more numerical analyses are executed on a new modified model. In this model resin's Young Modulus is increased (3 times larger) in order to increase the rigidity of steel-CFRP connection. The results (Figure 2.35) indicate that resin's characteristics strongly affect the total response, since both the maximum moment of resistance as well as the maximum CFRP stress increases.

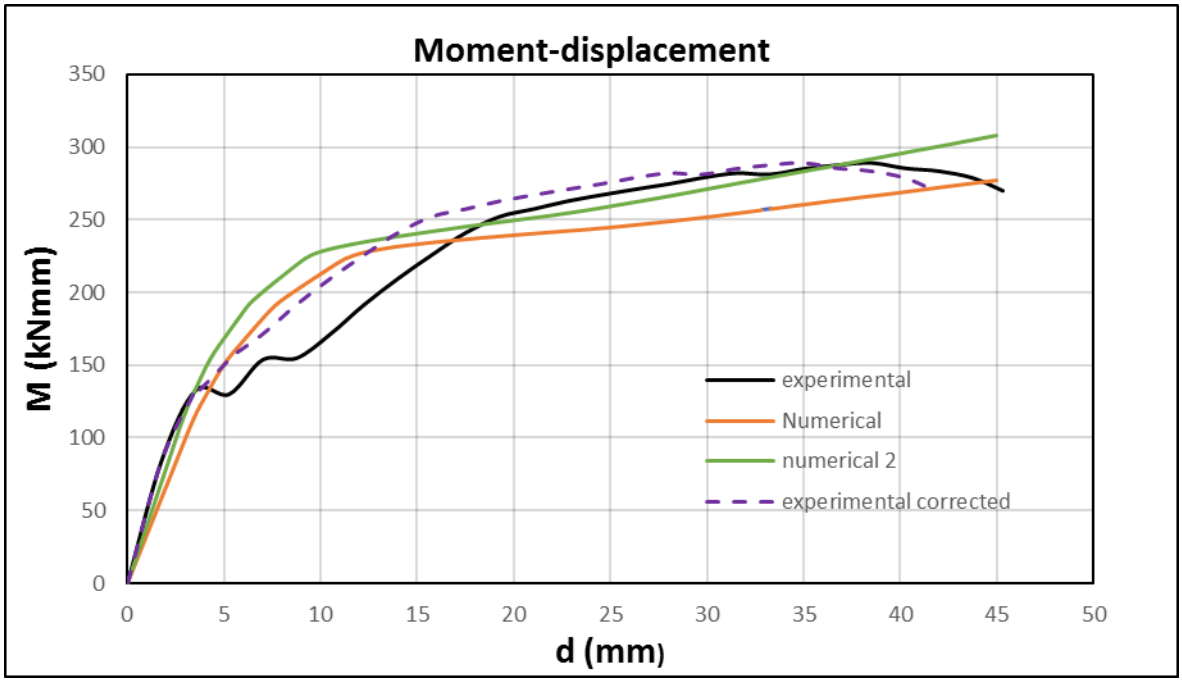

Figure 2.35: M-d curve for resin with larger stiffness

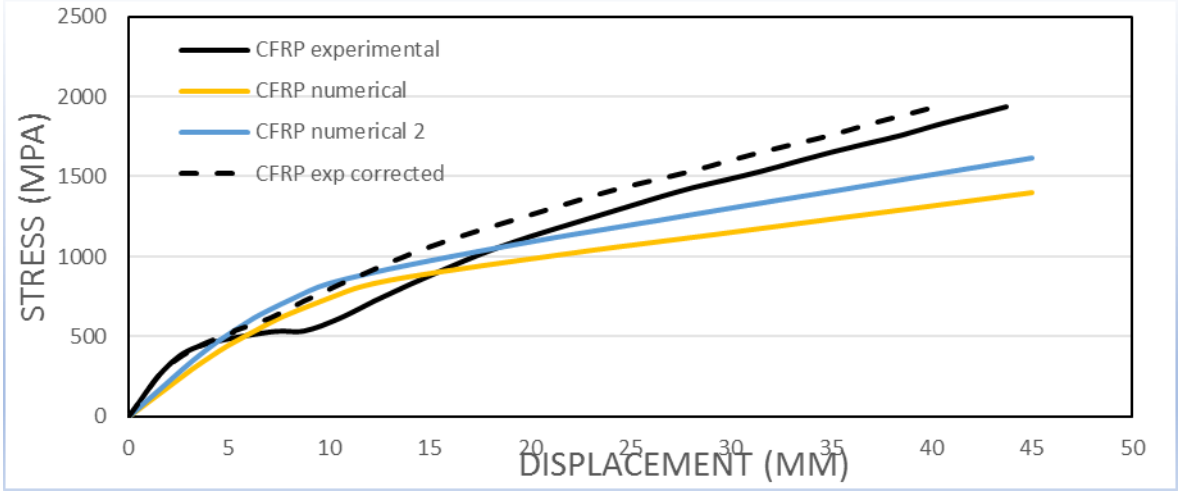

Figure 2.36: CFRP σ-d curve for the new model

2.5 Four-point bending test (CFRP plate on the compression side)

2.5.1 Testing set-up

The set-up for this test is shown in Figure 2.37. It is the same as the previous test. The only difference is that the CFRP plate is placed on the compression side of the specimen. The load was applied via displacement control with a speed of 0.420 mm/min. Figure 2.38 shows the specimen before and during testing. Two stain gauges were assigned on both sides of the specimen (on steel and CFRP) to measure the materials' strain. The total load and the specimen's deflection was also measured during the test.

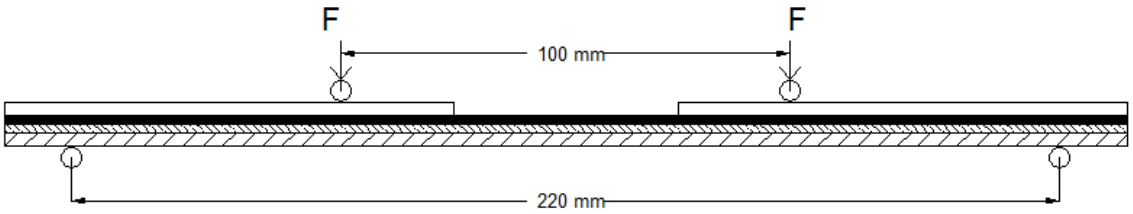

Figure 2.37: Testing set-up for the 3nd specimen

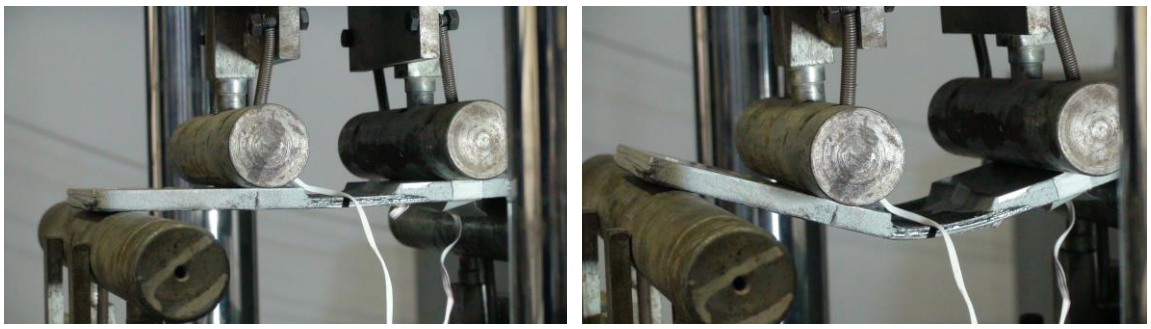

Figure 2.38: Specimen before and during testing (CFRP on the compression side)

2.5.2 Test results

The specimen exhibits an inelastic response with large plastic strains. Its response is similar to the previous specimen tested. Small slip was also indicated at certain times during the test. The force-displacement diagram of the test is shown in Figure 2.39. Using

Eq. 2.3 for the calculation of bending moment, the M-d diagram is calculated (Figure 2.40). shows the stress-strain curves for the two materials, measured by the strain gauges. It must be noticed that CFRP's strain data were not recorded until the end of the test, because the strain gauge at the compression side of the specimen was disconnected due to large strain.

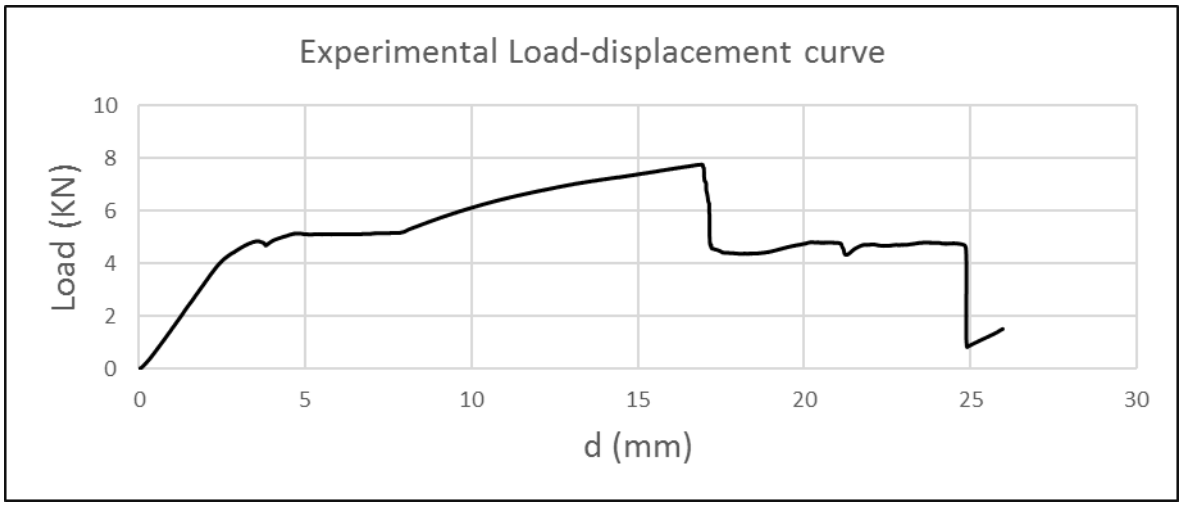

Figure 2.39: Test load-displacement curve

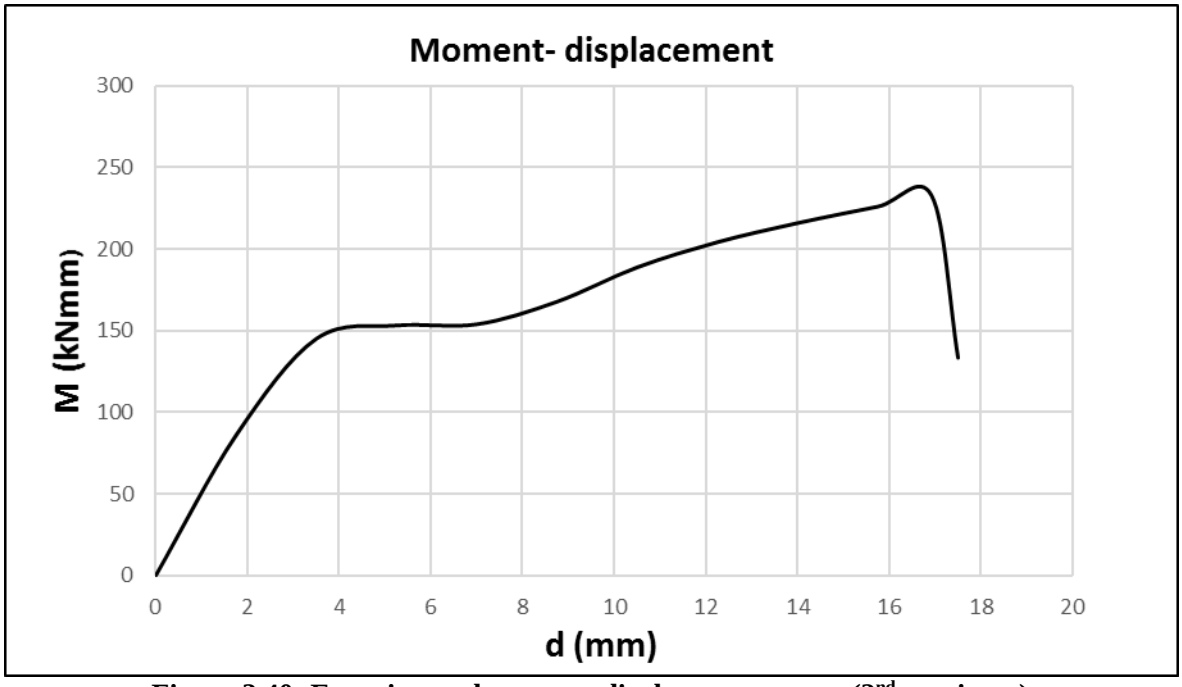

Figure 2.40: Experimental moment-displacement curve (2nd specimen)

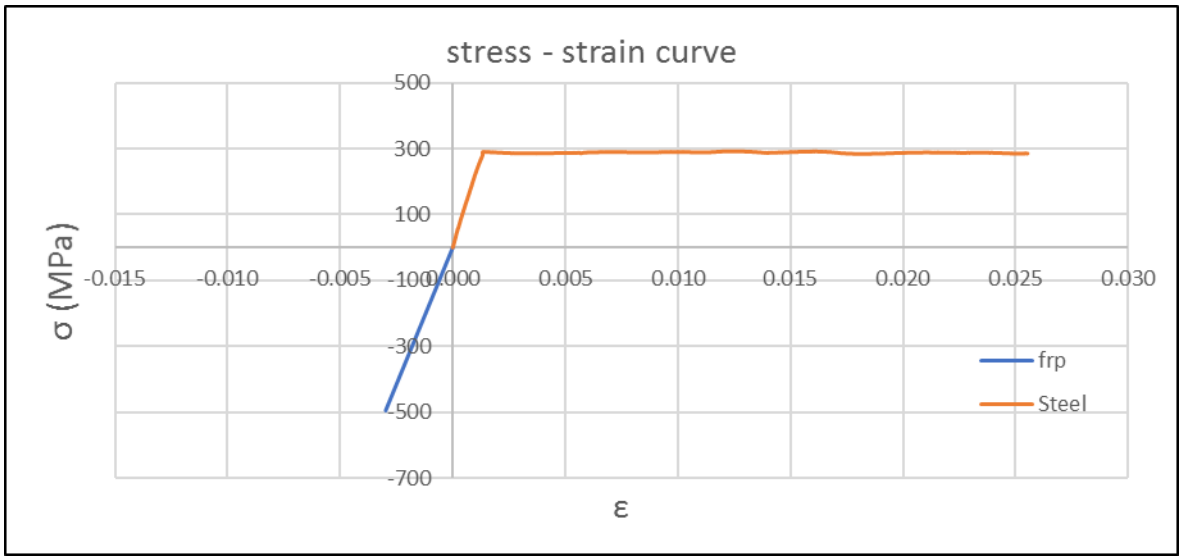

Figure 2.41: Experimental material σ-ε curves

2.5.3 Analytical calculations

Following the calculation process that is described analytically in Paragraph 2.4.3, composite section's moment resistance is estimated and is compared with the experimental values. The two different methodologies described in this paragraph are used again. As in the previous test, strain data in the compression side are recorded until the end of the test.
In addition to the two analytical methodology, in this test also a third method was used. In the third calculation method, it is considered that CFRP stress is constant over the height of CFRP's section, not linearly distributed. This assumption is made because the compression part of the section is very small, actually only the CFRP is in compression, since resin is ignored.

Comparing Experimental-Analytical results

A comparison between experimental results and analytical calculation of section's resistance moment (with all methods) is shown in Figure 2.42. It is noticed that all methods estimate smaller moment resistance values. The best match seems to be with results based on the third method. Despite the missing data using method 2 a good prediction of the section's response can be made. What is crucial is to estimate the ultimate compression strength of the CFRP plate. Base on the analytical procedure this strength is estimated to 640 Mpa.

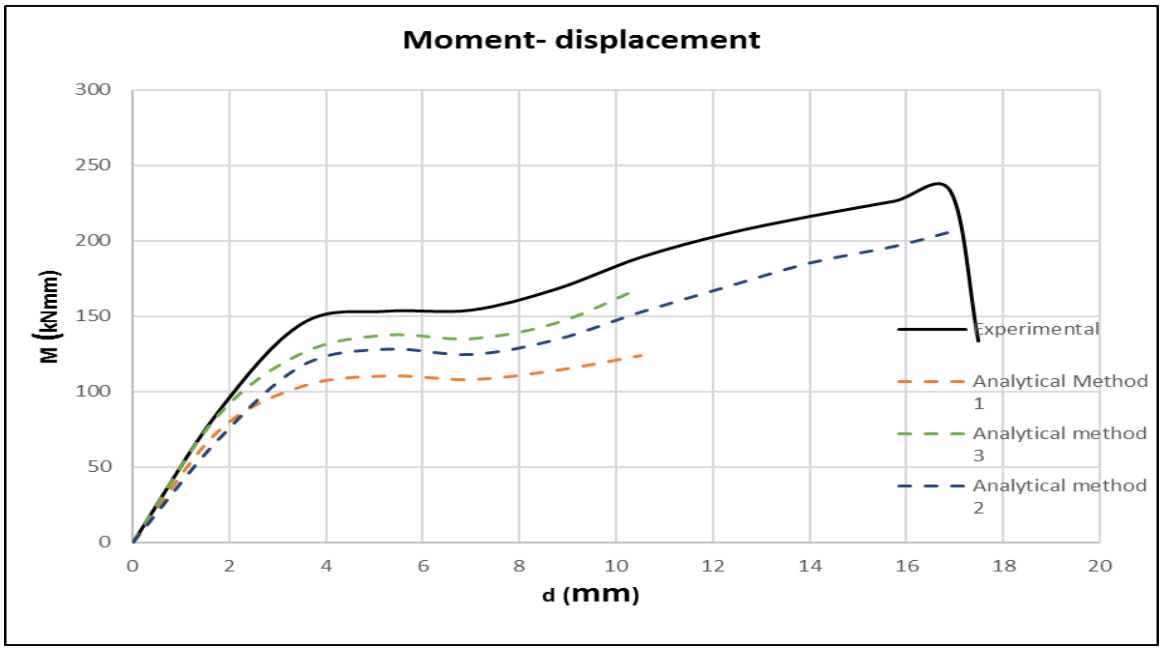

Figure 2.42: Analytical M-d curve for the second specimen

2.5.4 Numerical results

In this paragraph the results from the numerical analyses are presented. As mentioned in Paragraph 2.2.4 two main analyses are executed, both regarding non linear material but only the second takes account nonlinear geometry. Figure 2.43,Figure 2.44 and Figure 2.45 show the deformation and the strain distribution on steel and CFRP plate.

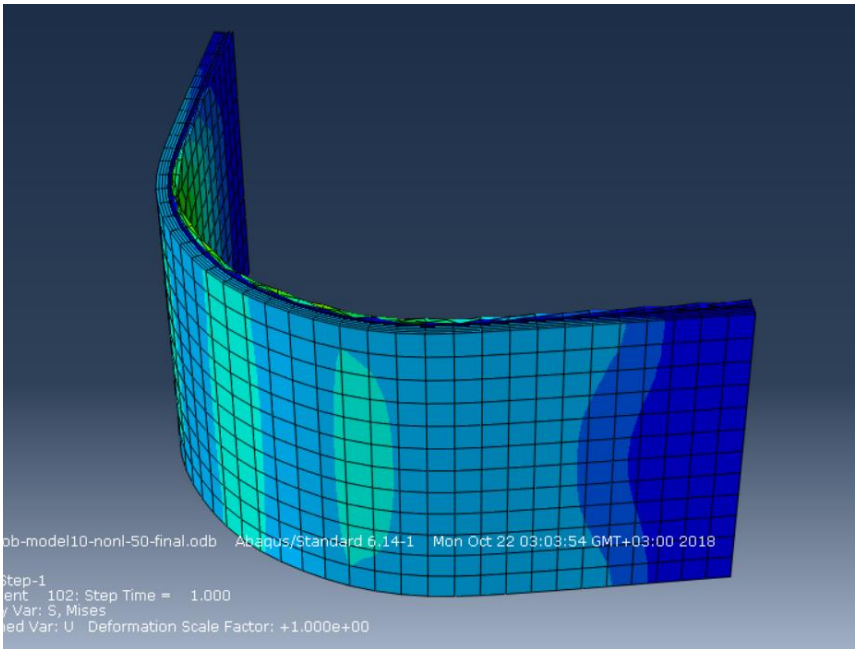

Figure 2.43: Deformed shape for the 2nd model

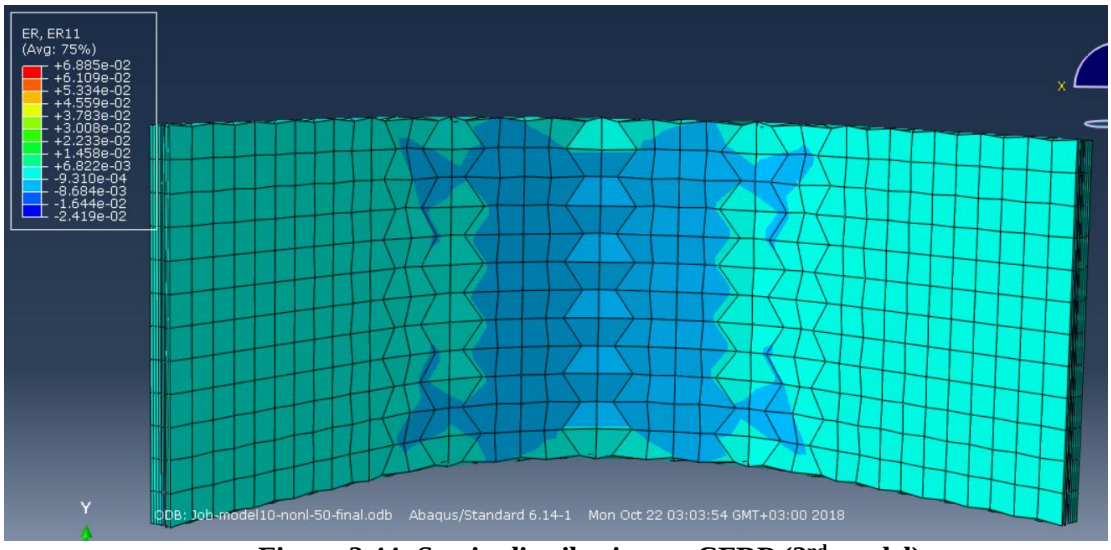

Figure 2.44: Strain distribution on CFRP (2nd model)

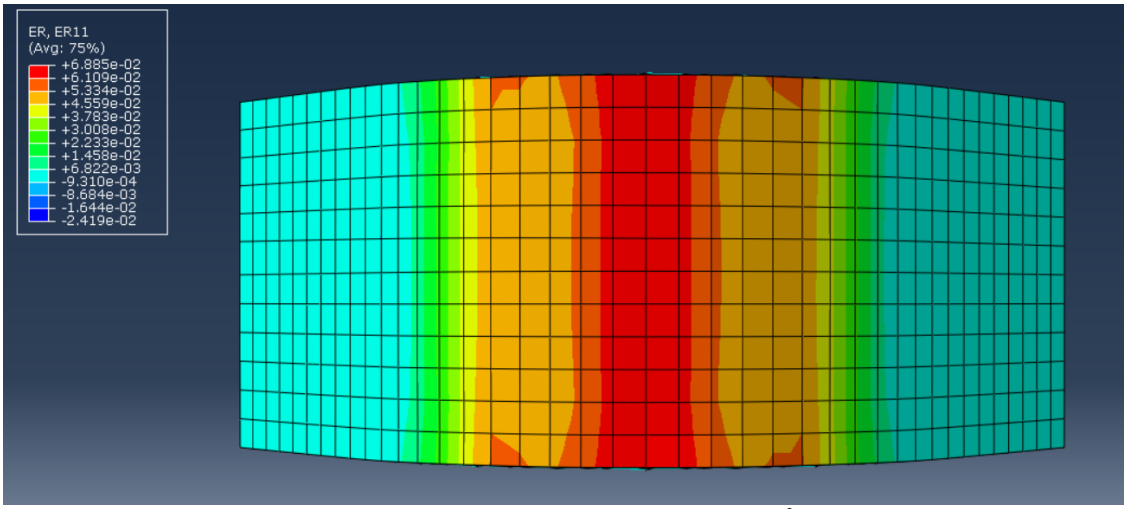

Figure 2.45: Strain distribution on Steel (2nd model)

Figure 2.46 shows the moment-displacement curve that occurred by the numerical analyses. As it is noticed the nonlinear model's curve matches better the experimental curve. Regarding the ultimate resistance moment, numerical models cannot calculate it because CFRP material is considered as a linear material, without any limitation in its compression strength. So it expected the numerical curve to have a large plastic part, which is unrealistic since CFRP fails earlier. As it was mentioned before, a small slip was observed during the test. This is noticed in the experimental M-d curve and probably causes some deviation between the experimental and the numerical curves. A new corrected M-d curve (Figure 2.47) is calculated after removing the observed slip, to make a better comparison between the curves.

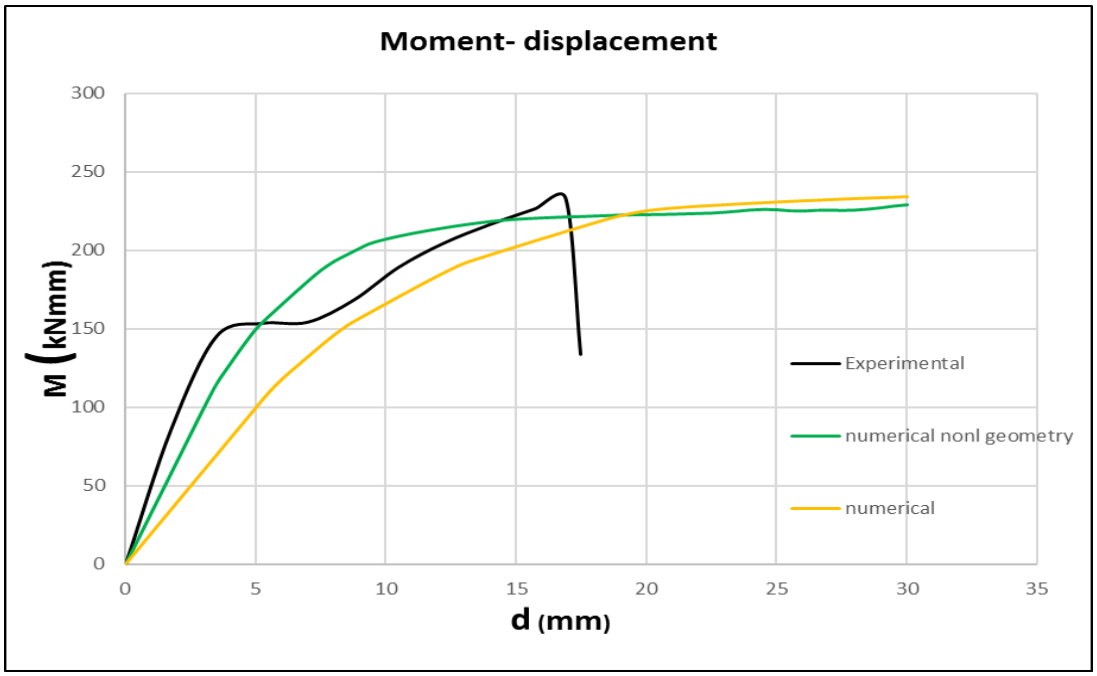

Figure 2.46: Numerical M-d curves

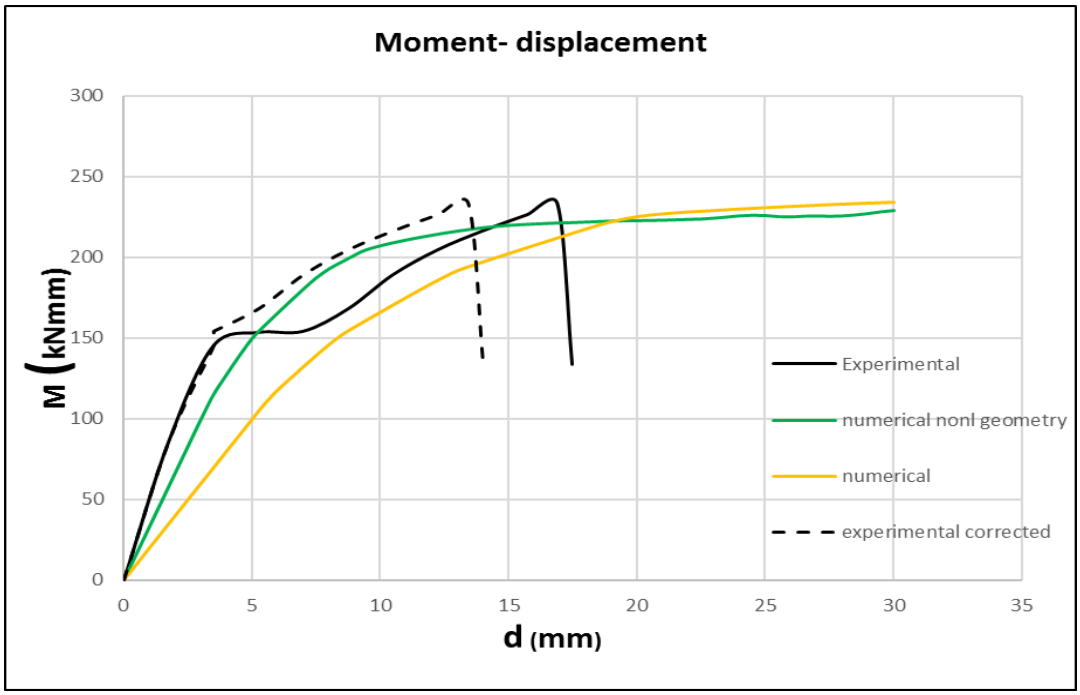

Figure 2.47: Corrected experimental M-d curve

Figure 2.48,Figure 2.49, and Figure 2.50 show the numerical stress-strain and stress displacement curves compared with the experimental results. It is noticed that the numerical CFRP s-d curve differs than the experimental. The CFRP material at the numerical model is elastic, without any strength limitation, which obviously is not real. For this reason, based on the experimental test and the ultimate displacement. It is estimated that CFRP fails approximately at 700Mpa, which is a value near to the numerical one (630 MPa)

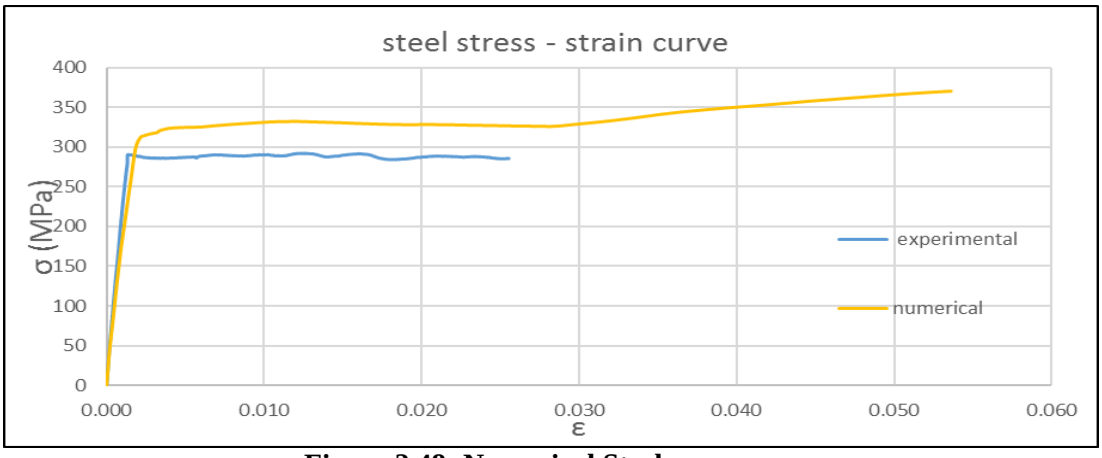

Figure 2.48: Numerical Steel σ-ε curve

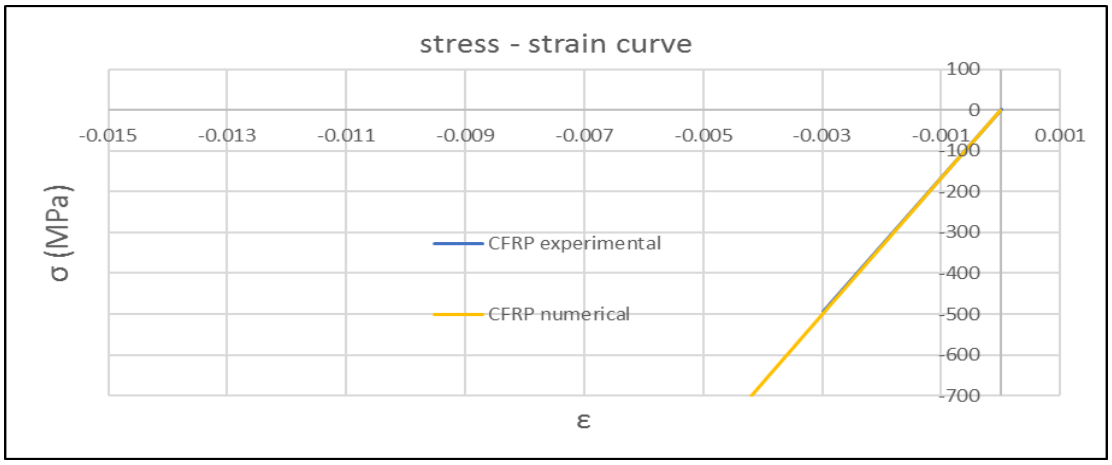

Figure 2.49: Numerical CFRP σ-ε curve

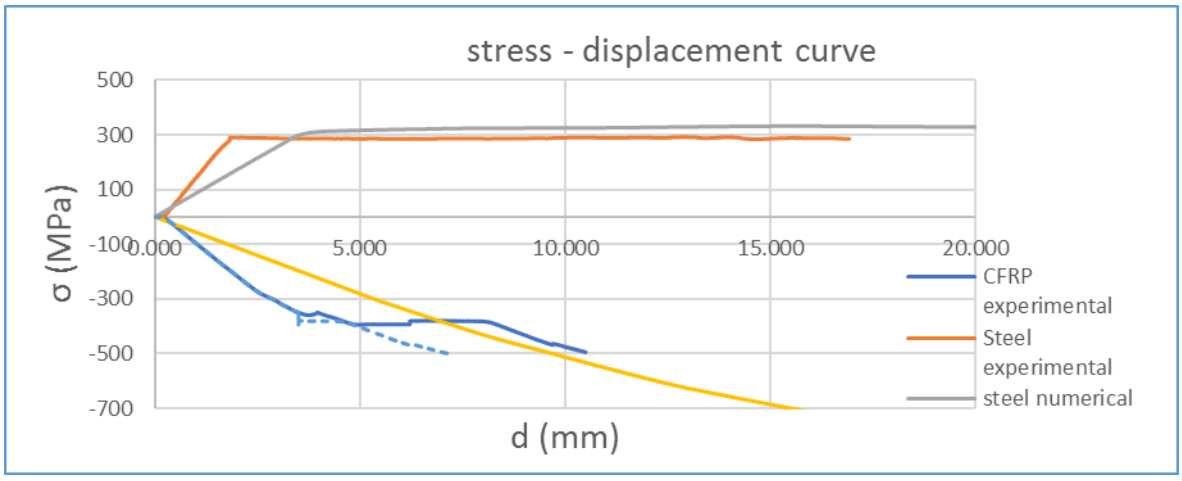

Figure 2.50: Numerical stress-displacement curves

2.6 Conclusions

Based on the experimental tests it is concluded that strengthening steel plates with CFRP is a very effective method, which increases the axial capacity and the resistance moment of steel sections, even in case CFRP plates are used under compression. Figure 2.51 shows that the two specimens exhibit the same response, independently if the CFRP was in tension or in compression side. Actually, the ultimate resistance moment of the 2st

specimen is 20% larger than the 3rd . It is impressive, that comparing the strengthened steel plate with a steel plate alone, is concluded that CFRP strengthening increased bending capacity of the plate almost 5 times. In addition, in the case of the 2nd specimen a large amount of plastic deformation capacity is verified. Also, as it is concluded on the previous paragraph an assumption can be made about the compression strength of the CFRP plate, since usually there is no data about it. So, based on the above it can be estimated that CFRP's compressive strength may reach at a value of 700Mpa.

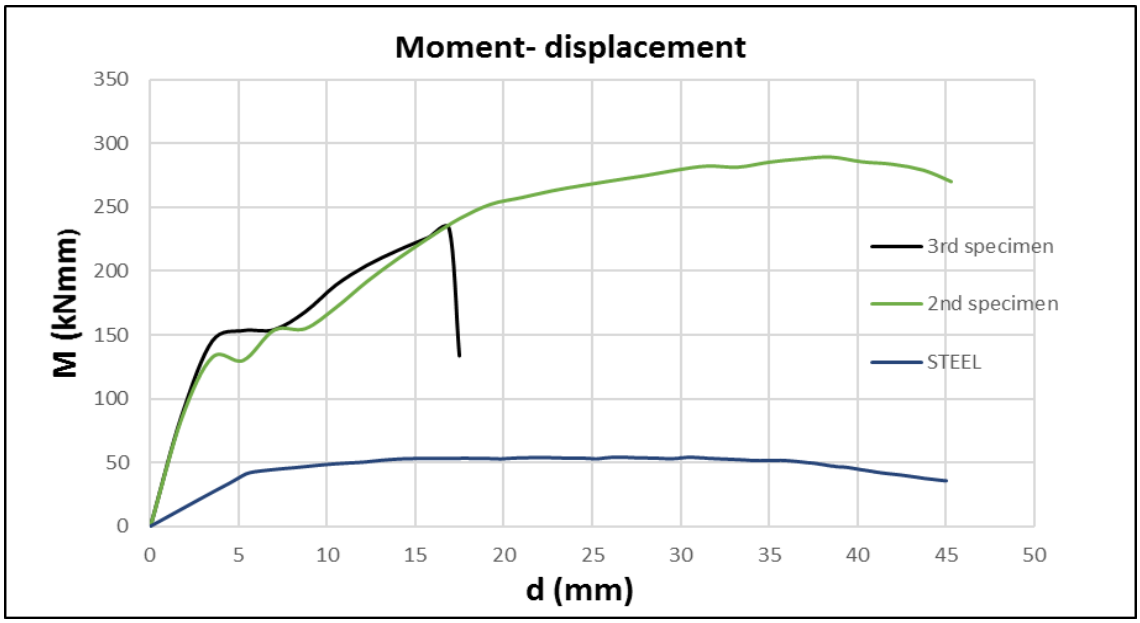

Figure 2.51: Comparison between the two specimens

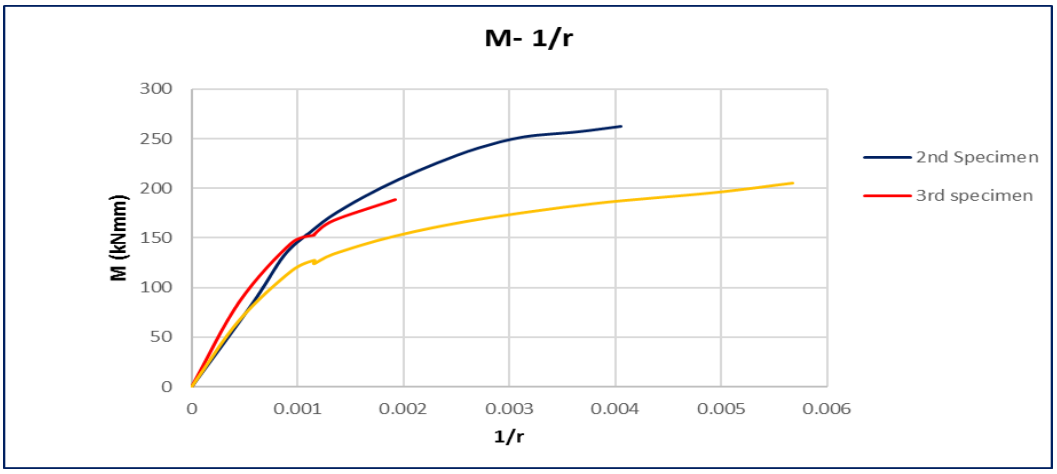

Figure 2.52: Comparison between M-1/r diagram for the two specimens

3 Analysis of an existing telecommunication tower

3.1 General

In the current paragraph the evaluation of a typical existing self-supporting lattice tower of the Cosmote telecommunication network is presented. For this study, the geometry of the structure is taken from the drawings provided by the telecommunication company. Further on, it is assumed that no corrosion or other adverse effect has altered the geometry or the mechanical characteristics of the material of the members.

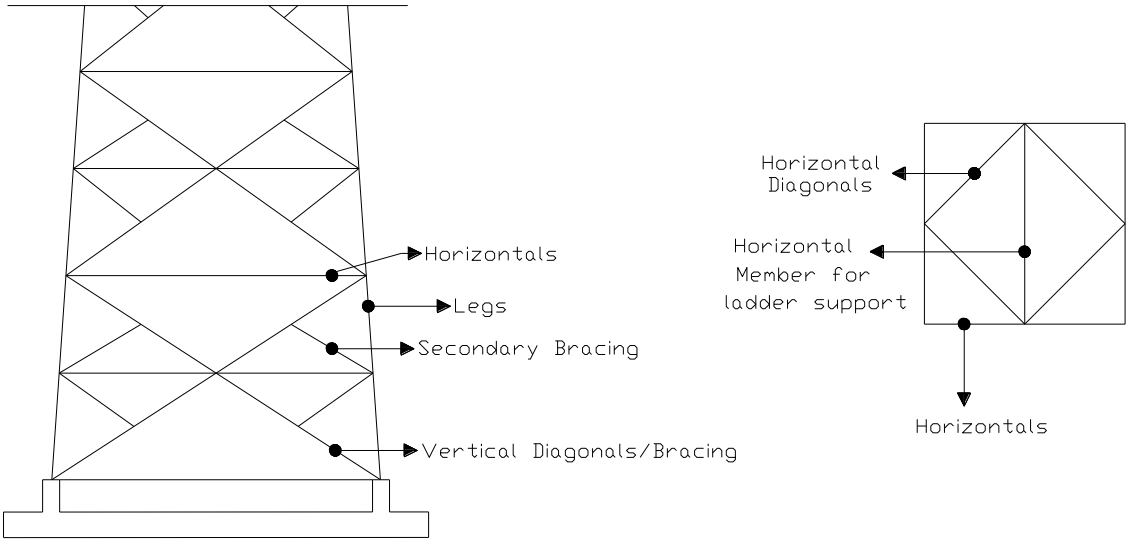

Figure 3.1: Designation of structural members

Materials

The Steel grade of the structural members is S235 according to EN 10025. The material's properties used for the structural analysis and design are shown in Table 3.1 and Figure 3.2 . The safety factor for the material is taken as $\gamma_m = 1.10$.

Table 3.1: Material's properties

Mat 1 S 235 (EN 1993)

Young's modulus	E	210000	[N/mm2]	Safetyfactor		1.10	[-]
Poisson's ratio	μ	0.30	[-]	Yield stress	fy	235.00	[MPa]
Shear modulus	G	80770	[N/mm2]	Compressive yield	fyc	235.00	[MPa]
Compression modulus	K	175000	[N/mm2]	Tensile strength	ft	360.00	[MPa]
Weight	γ	78.5	[kN/m3]	Compressive strength	fc	360.00	[MPa]
Density	ρ	7850.00	[kg/m3]	Ultimate strain		100.00	[o/oo]
Elongation coefficient	α	1.20E-05	[1/K]	relative bond coeff.		0.00	[-]
max. thickness	t-max	40.00	[mm]	EN 1992 bond coeff.	k1	0.00	[-]
				Hardening modulus	Eh	0.00	[MPa]
				Proportional limit	fp	235.00	[MPa]
				Dynamic allowance	σ-dyn	0.00	[MPa]

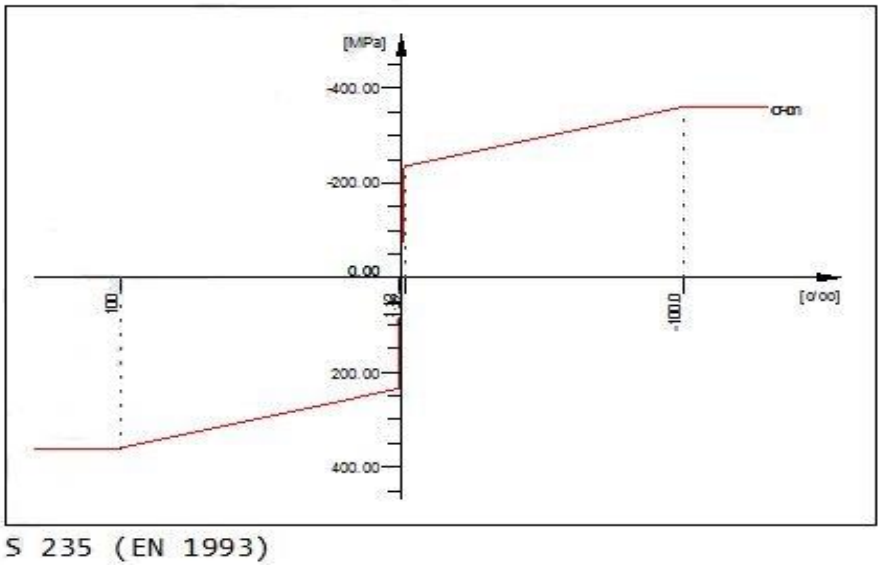

Figure 3.2: Material's stress-strain curve

Cross sections

The cross sections and the diaphragm of the structural system is shown in Table 3.2:

Table 3.2 : Cross sections of the tower

No		Type of member	Section
1	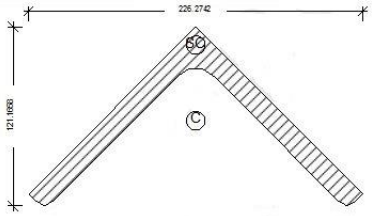	Legs at height 0 – 24 m	L160.15
2	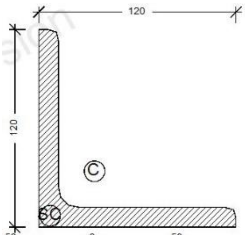	Legs at height 24 – 48 m	L120.12
4	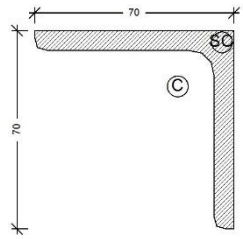	Vertical bracing system and members at the top of the tower	L70.7

5	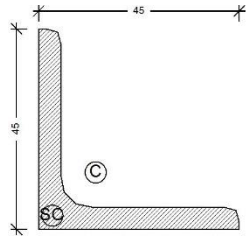	Secondary vertical bracing system and horizontal bracing system (except from levels with resting platforms)	L45.5
6	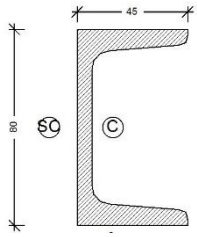	Horizontal bracing system at levels with resting platforms (heights 12, 24, 36, 42, 45 m)	U80
7	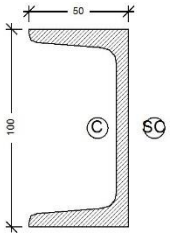	Horizontal members	U100
8	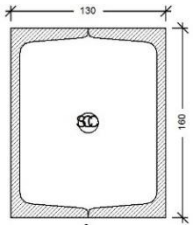	Central Horizontal members These members bear the loads of the ladder, the waveguide rack and the cables	2 x U160 welded on both edges

3.2 Loads and Load Combinations

For the study of the lattice tower, the following permanent and variable loads are taken into account:

3.2.1 Permanent Loads

- **Self-weight of steel structure**

The self-weight is calculated by the analysis program considering the specific weight of steel γ=78.50 kN/m^3

- **Weight of climbing ladder, waveguide rack and cables, lightning rod**

The weight of the climbing ladder is equal to 0.153 kN/m . The weight of the waveguide rack is equal to 0.146 kN/m .
In addition, a lightning rod Φ48.3*3.2 with length of 1.25 m and a weight of 0,045kN is taken into account, placed on the top of the tower.

- **Self-weight of working platforms**

Working platforms are located at +12.00, +24.00, +36.00, +42.00 and +45.00m height. The weight of each platform is equal to 0.235kN/m^2.

3.2.2 Live Loads

- **Live Load of climbing ladder**

The live load of the climbing ladder has been taken equal to **1 kN/m** .

- **Live Load of working platforms**

The live load of the working platforms has been taken equal to **2 kN/m^2 .**

3.2.3 Ice load

For the calculation of ice load, it is assumed that all structural members, components of ladders, ancillaries etc are covered with ice having a thickness of 30mm over the whole surface of the member. (Ice density has been taken equal to 7.00 kN/m^3). Thus, i.e. the ice load for the parabolic antennas is calculated based on the following formula:

$$G_S = \frac{\pi \times a}{2} \times \left[2 \times b \times (\Phi + a) + (\Phi + 2 \times a)^2\right] \times \gamma_{ice} \quad , [kN]$$

Eq. 3.1

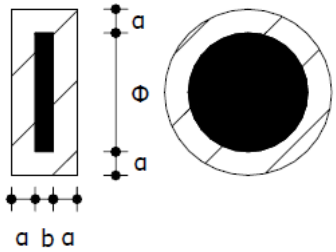

3.2.4 Wind

Based on Eurocode 1 and the Greek National Annex the basic wind speed for the study is taken equal to 33m/sec, since the structure is located in an area with distance from the sea smaller than 10km.

'<u>Gust' wind load</u>

The gust wind force acting on the incremental area j of the structure at the height z_j is determined from:

$$F_{t,w}(z_i) = F_{m,w}(z_i)\left(1 + \frac{1 + 0.2\left(\frac{z_i}{h}\right)^2}{c_o(z_i)}\left[(1 + 7I_v(z_i))c_s c_d - 1\right]\right)$$

Eq. 3.2

where:

$F_{m,w}$ is the mean wind load force

c_s c_d is the structural factor, taken as 1.

z_j height of the center of gravity of incremental area A_j

$I_v(z_i)$ turbulence intensity at height z_i

$c_0(z_i)$ orography coefficient at height z_i

Mean wind load

The mean wind force acting on the structure is determined from a summation of pressures acting on surfaces. The mean force F_{wj} acting on the incremental area j at the height z_j is:

$$F_{m,w}(z_i) = \frac{q_p}{1+7I_V(z_i)} \sum c_f A_{rcf} \qquad \text{Eq. 3.3}$$

where:

q_P is the basic velocity pressure

c_f force coefficient for incremental area A_j

z_j height of the centre of gravity of incremental area A_j

A_{ref} Reference area

$I_v(z_i)$ turbulence intensity at height z_i

The basic velocity pressure at the height z_j is:

$$q_p(z_i) = [1 + 7 \cdot I_v(z_i)] \cdot \frac{1}{2} \cdot \rho \cdot v_m^2(z_i) \qquad \text{Eq. 3.4}$$

where:

v_m is the mean wind velocity

ρ is the air density (equal to 1.25Kg/m^3)

z_j height of the center of gravity of incremental area A_j

$I_v(z_i)$ turbulence intensity at height z_i

The mean wind velocity at the height z_j is:

$$v_m(z_i) = c_r(z_i) \cdot c_o(z_i) \cdot v_b \qquad \text{Eq. 3.5}$$

where:

v_b is the basic wind velocity

$c_r(z)$ is the roughness coefficient

$c_o(z)$ is the orography coefficient

z_j height of the center of gravity of incremental area A_j

The basic wind velocity, defined as a function of wind direction and time of year at 10m above ground of terrain category II, is:

$$v_b = c_{dir} \cdot c_{season} \cdot v_{b,0} \qquad \text{Eq. 3.6}$$

where:

$v_{b,0}$ is the fundamental value of the basic wind velocity, taken as **33.00m/sec**.

c_{dir} is the directional factor, taken as 1.

c_{season} is the season factor, taken as 1.

Due to symmetry, two wind directions, 0^0 (W_o) and 45^0 (W_l) were considered. For the two wind directions, the total wind load is distributed on each side of the tower according to Table 3.4:

Table 3.3: Table of wind rates to the surface

		I	II	III	IV
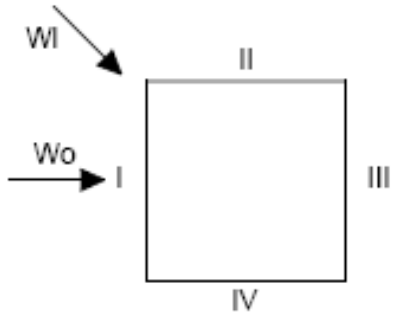	W_o vertical to surface	57%	0%	43%	0%
	W_o pararell to surface	0%	0%	0%	0%
	W_l vertical to surface	20%	20%	15%	15%
	W_l pararell to surface	20%	20%	15%	15%

3.2.5 Antennas

Design loads are given in paragraph 1.4. In addition to those four parabolic antennas with a diameter of 2.40m are assumed on each side of the tower, at the top (height 45-48m).

Weight of parabolic antennas

The parabolic antennas are placed on the tower through a special designed system. The system is made of 12mm thick hot-dip galvanized steel plates with a length of 3.00m. The length of the support arms is 0.50m. Each antenna weighs 2.3 kN.

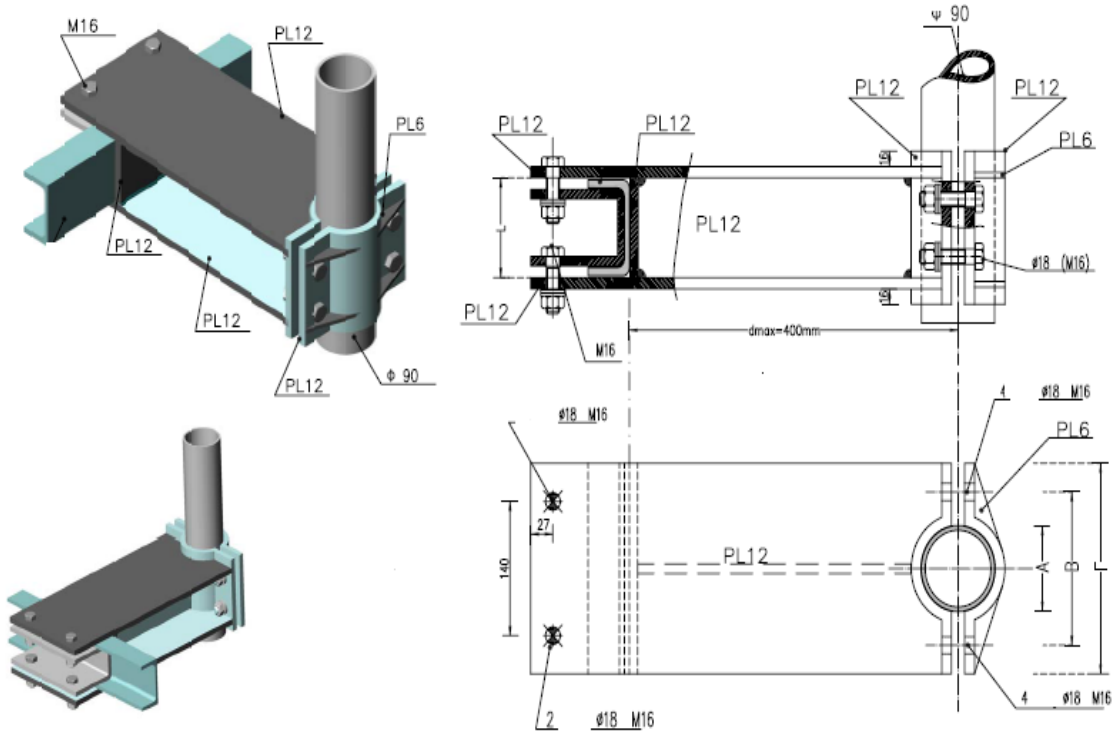

Figure 3.3: Antenna Support system placed at the horizontal UPN members of the tower

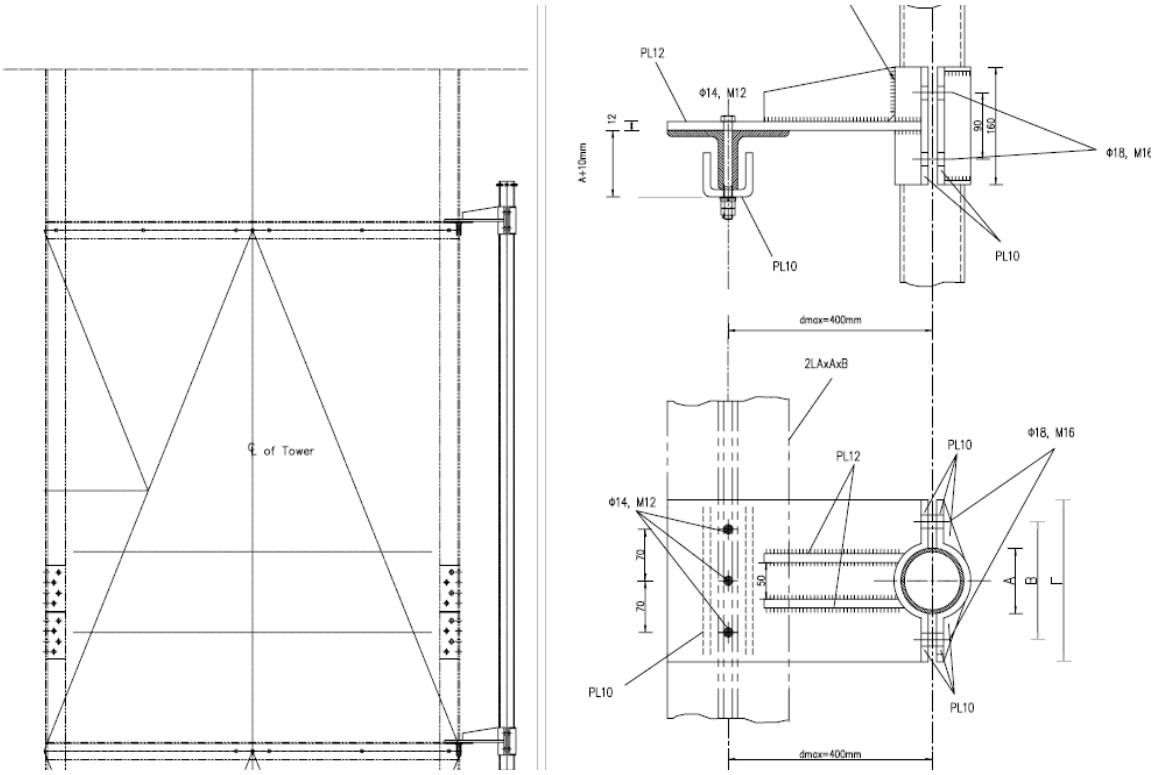

Figure 3.4: Antenna Support system placed at the horizontal double angle members of the tower

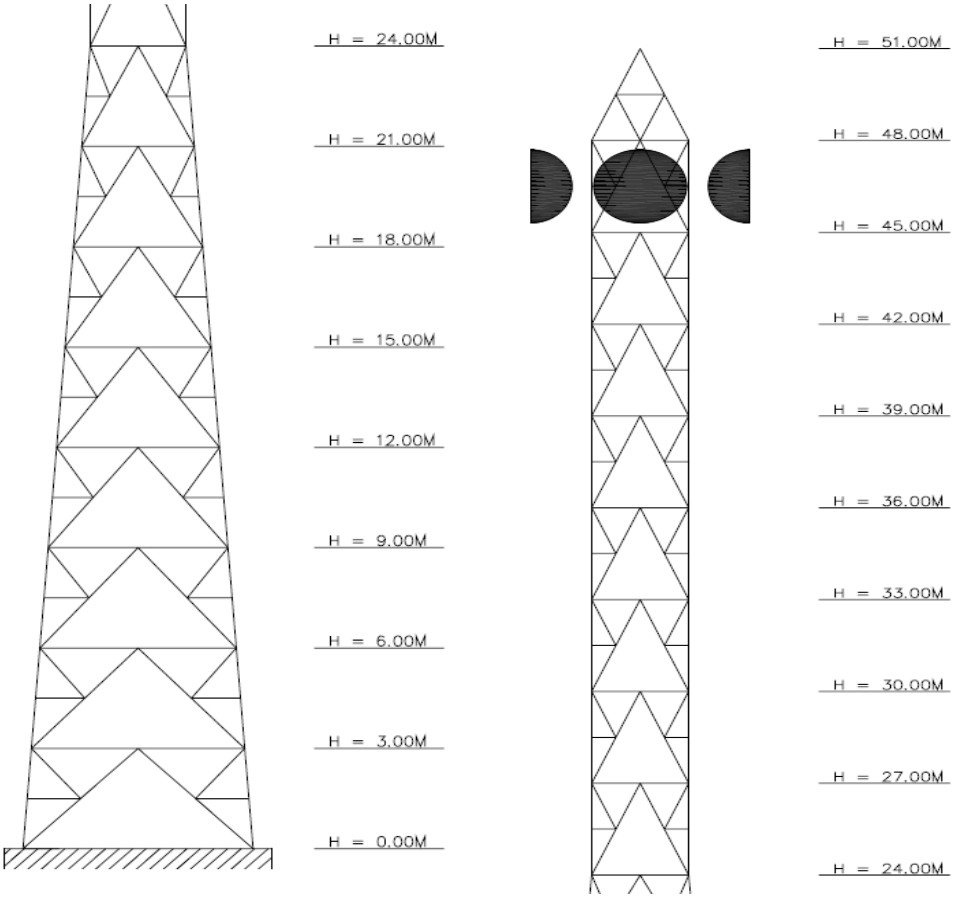

Figure 3.5: Position of parabolic antennas on tower

Wind Load on parabolic antennas

The wind load on the parabolic antennas is calculated with the use of the freeware software Andwind. Force (F_A) acts along the axis of the antenna, side force (F_S) acts perpendicular to the antenna axis and the twisting moment (M) acts in the plane containing F_A and F_S.

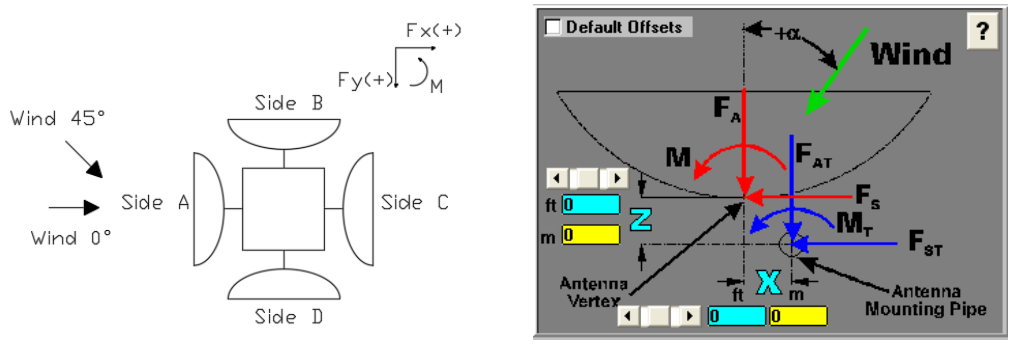

(a) **(b)**

Figure 3.6: (a) Configuration of the parabolic antennas on the tower and (b) depiction of the wind forces acting on a parabolic antenna

The wind forces on a 2.40 m diameter parabolic antenna are given in Table 3.4.

Table 3.4: Wind forces for a 2.40 m diameter parabolic antenna located at 45m height

Side	Angle θ of the wind loading	F_a (kN)	F_s (kN)	Moment (kNm)
A	**0º**	9.060	0.000	0.000
	45º	8.050	2.104	-0.712
B	**0º**	4.490	-0.790	-1.720
	45º	2.104	8.050	0.712
C	**0º**	7.300	0.000	0.000
	45º	6.440	1.950	-1.500
D	**0º**	4.490	0.790	1.720
	45º	1.950	6.440	1.500

3.2.6 Earthquake

The earthquake loading is calculated in accordance with Eurocode 8. For the modal analysis the following parameters have been taken into account:

- Peak ground acceleration, a = 0.24g
- Importance factor, $\gamma = 1.40$
- Behavior factor, q = 1.00
- Soil class B
- Modal damping 4%

3.3 Modelling for analysis

The tower was modelled and analysed using the SOFISTIK finite element software. The tower members are simulated as by means of 6DOF beam elements. Some major design assumptions are summarized below:

- Hinges are assigned to the ends of all braces and horizontal members.
- There is no eccentricity in beam's connections, all members are simulated as centric beam elements.
- The foundations for the legs are modelled as pinned supports.

Characteristic pictures of the numerical model are shown in Figure 3.7.

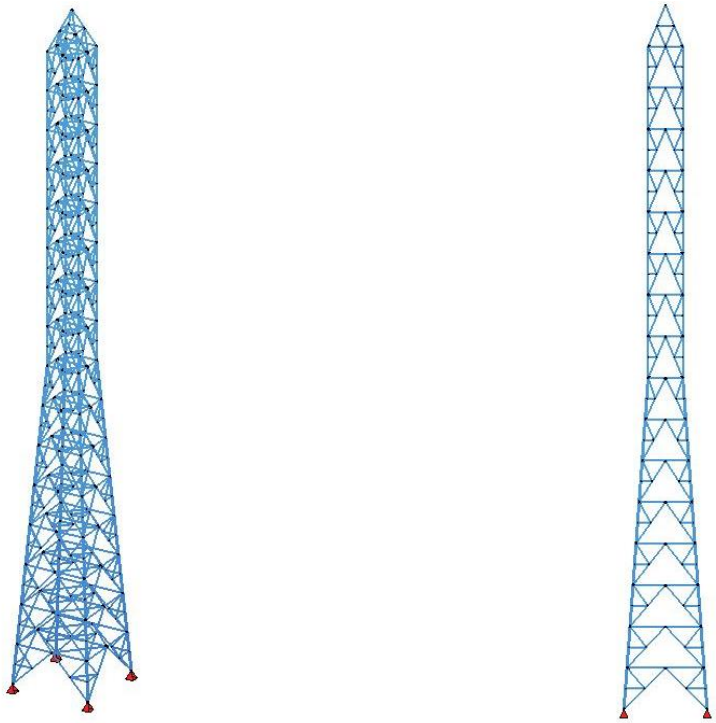

(a) (b)

Figure 3.7: Three-dimensional structural model used for the analysis of the tower: a) prospective view b) side view

3.4 Global Analysis and design

At first, Modal Analysis was performed to determine the natural frequencies of the tower. The first modes and the corresponding periods are shown in Figure 3.8. Due to structure's

and loads' symmetry the first two modes have the same period but refer to different (major) direction. The 3rd mode is torsional.

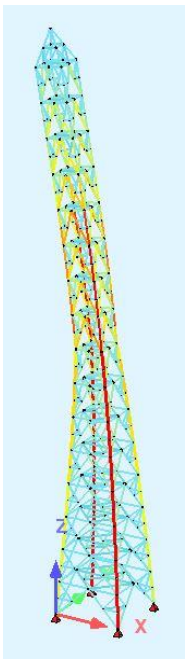

1st mode

T = 0.925 sec

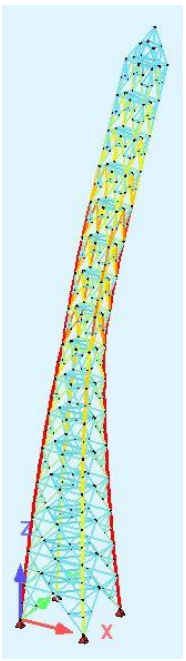

2nd mode

T = 0.925 sec

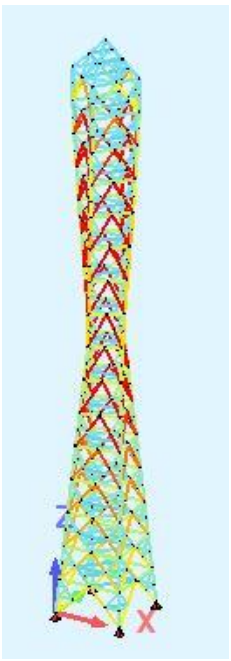

3rd mode (torsional)

T = 0.25 sec

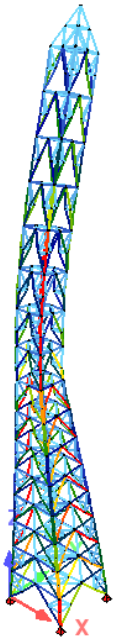

4th mode

T = 0.226 sec

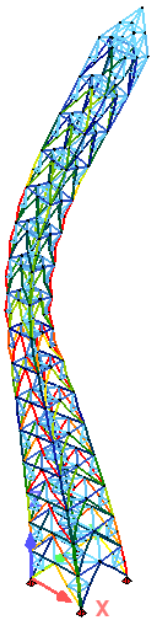

5th mode

T = 0.226 sec

Figure 3.8: First Modes

Table 3.5: Tower's Modes

Modal masses - activated masses								
mode	Period	modal mass			modal mass factor			activated
	[sec]	X[t]	Y[t]	Z[t]	X[%]	Y[%]	Z[%]	mass [%]
1	0.929	11.32	3.59	0	37.47	11.87	0	19.441
2	0.929	3.59	11.31	0	11.88	37.44	0	19.432
3	0.251	0	0	0	0	0	0	22.187
4	0.226	1.35	7.76	0	4.48	25.67	0	28.324
5	0.226	7.77	1.35	0	25.72	4.46	0	29.185
	SUM	27.89	27.85	0	92.31	92.18	0	

Ultimate Limit State (ULS)

Global analysis was followed by structural design, where all members are checked in accordance with EN 1993-1-1 and EN 1993-3-1 using the software package SOFISTIK. For each tower's member the utilization factor against flexural buckling to compression and bending (FLB), lateral torsional buckling (LTB) and buckling to pure compression (buckling) is calculated at Ultimate Limit State (ULS). The utilization factor for full exploitation of the cross-section is 1.0 (100%). Larger values indicate no permissible overloading of members, which means that the mentioned member does not cover the required regulations. Rates less than 1.0 suggest that the member could receive more loads. In Table 1.5 the maximum utilization factors are given for each member type of the tower. In Figure 3.9 the members that are overloaded are highlighted in red.

Table 3.6: Maximum utilization factor for each member type

Member's type	Maximum utilization factor	Overloading in segments
Legs	1.95	0-33m
Vertical braces	1.61	0-12m and 24-36m
Horizontal members	0.75	
Secondary bracing members	0.76	
Horizontal braces	0.67	
Members supporting climbing ladder	0.19	

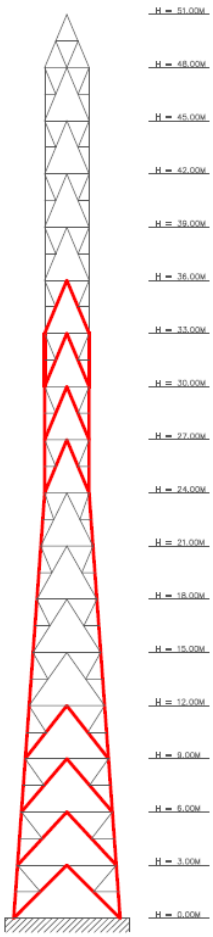

Figure 3.9: Overloading members

Serviceability Limit State (SLS)

The varication criteria for the tower at Serviceability Limit State (SLS) includes the calculation of the antennas vertical angle. The limit value is 0.5 degrees. Larger angle's values are not accepted because in this case antennas are not functional.

Figure 3.10 shows the deformed shape of the tower, enlarged by 20 for better display, as well as the horizontal displacement at each level. The maximum displacement at the top of the tower is 432 mm and it occurs for the 45º wind loading. The vertical angle of the parabolic antennas is calculated as following and is equal to 0.795 degrees, which is 60% larger than the limit value.

$$\varphi = \tan^{-1}\left[\frac{\delta_{top} - \delta_{bot}}{h_{bay}}\right] = \tan^{-1}\left[\frac{391.6 - 350}{3000}\right] = 0.795$$

where:

δ_{top} is the displacement at height +48m (upper side of antenna) and is equal to 391.6 mm
δ_{bot} is the displacement at height +45m (down side of antenna) and is equal to 350 mm
h_{bay} is the height of each bay of the tower and is equal to 3000 mm

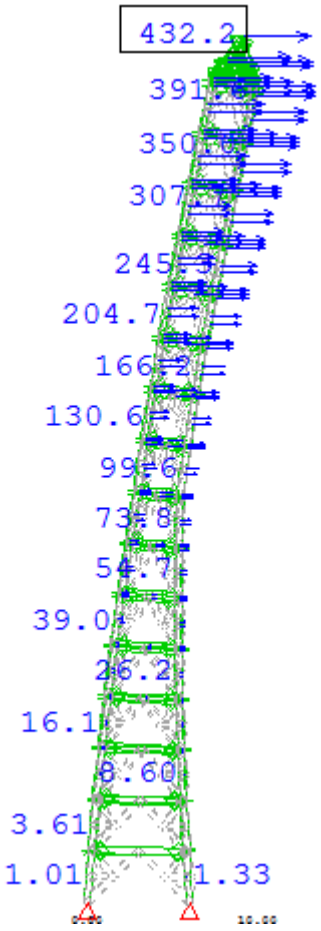

Figure 3.10: Tower's deformed shape and horizontal displacements at each level

3.5 Conclusions

As it concluded, the existing telecommunication tower cannot bear the extra load that correspond to bigger antennas. There is evaluated an overloading in legs until the height of +33m and at vertical braces at heights 0-12m and 24-36m. Also, the tower doesn't meat the code's requirements at SLS. That means that this tower need to be strengthened in order to fulfil latest code's requirements and future telecommunication needs. The main parts of the tower that seem to be the "weakest" are indicated in black square in Figure 3.11.

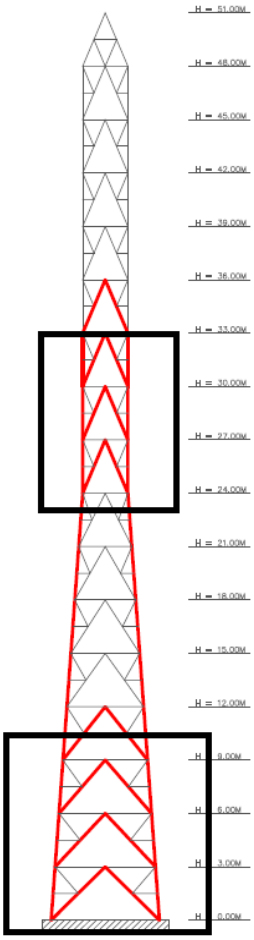

Figure 3.11: Tower's 'weakest'parts

4 Analysis and design of the tower with CFRP strengthening

4.1 General

This paragraph concerns the design of a tower, same as the initial tower described in paragraph 3, strengthened using plates made from Carbon Fiber Reinforced Polymer (CFRP plates).

Materials

As it is mentioned in paragraph 1.3 the steel grade for all members of the tower is S235, with material safety factor 1.10.

For the strengthening of the tower Carbon Fiber Reinforced Polymer plates (CFRP plates) are used having various widths and thickness of 1.2 mm. Regarding the modelling, it is considered that the CFRP material is a linear material with properties as seen in Table 4.1. Regarding the compression strength of CFRP material, the previous results are used to make an assumption. Because of the limited tests done, the compression strength that was calculated is used with safety factor 3.

Table 4.1: CFRP material's properties

Young's Modulus (E)	165 GPa
Tensile strength	2900 MPa
Compressive strength	210 MPa
Ultimate strain	1.75 %

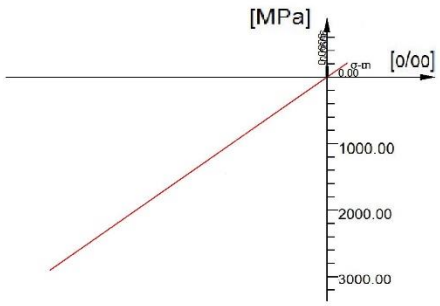

Cross sections

Strengthening of the tower is implemented by application of CFRP plates made from the material described in Table 4.1. The CFRP plates are applied only to members that need to be strengthened according to the previous analysis of the initial tower, as described in paragraph 3. More specifically, the legs of the tower are strengthened up to the level of 33m, the vertical braces up to the level of 42m and the rest of the members are not strengthened, since it is not needed. The number of CFRP plates that are used varies along the height of the tower. At the tower's base and at heights from 24 to 30m strengthening is executed with more plates than at the other parts, because in these parts the largest axial forces develop. Figure 4.1 shows in a picture how the strengthening is executed along the height of the tower for legs and braces.

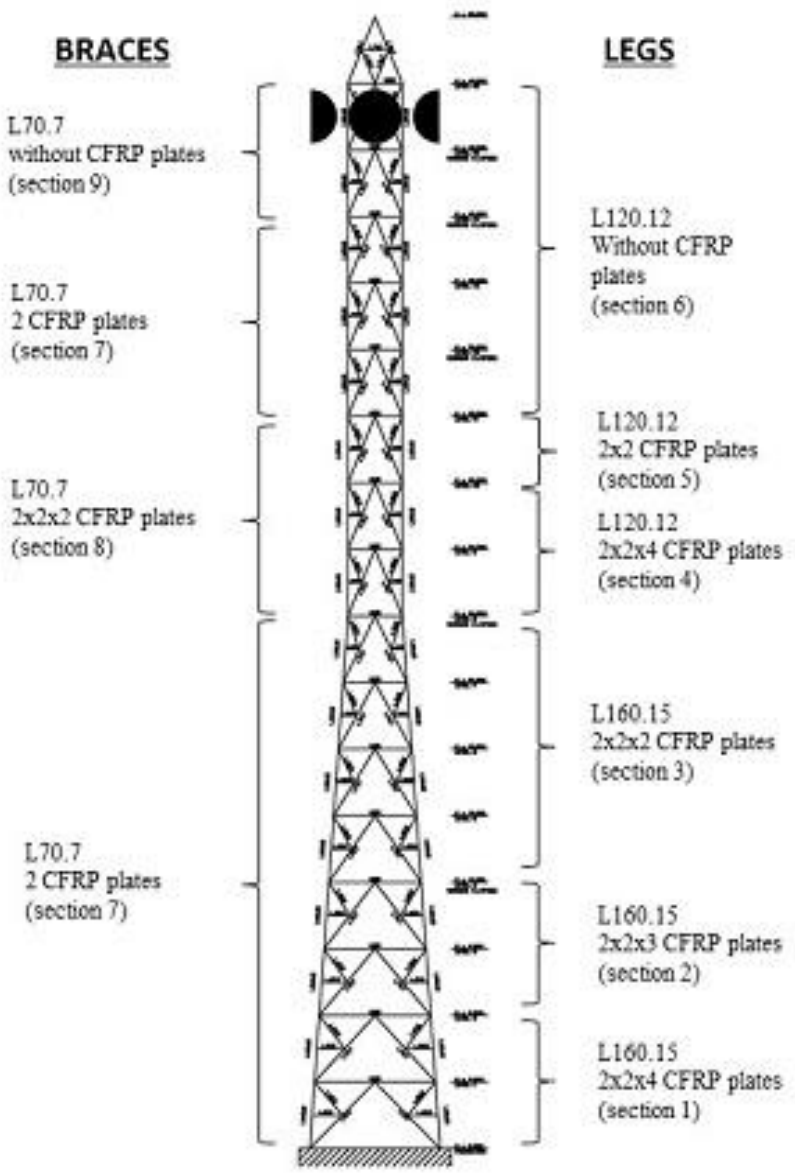

Figure 4.1: Tower strengthened with CFRP plates

All the various (strengthened or not) cross sections that are used, together with their position along the height are shown in Table 4.2 (Legs) and Table 4.3 (braces). These tables show also the width of the CFRP plates used, which varies from 50mm to 150 mm, and how they are applied to angle sections. The other members of the tower are the same as the members of the initial tower and are shown in Table 3.2 (Initial Tower).

Table 4.2 : Leg's cross sections

No	**Legs:**	Height	Section
1	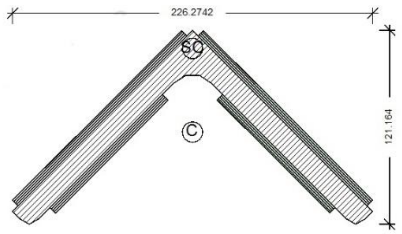	0 – 6 m	L160.15 (initial) 2x4 CFRP plates S1512 (150x1.2 mm) 2x4 CFRP plates S1012 (100x1.2 mm)
2	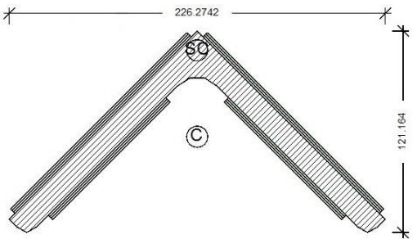	6-12 m	L160.15 (initial) 2x3 CFRP plates S1512 (150x1.2 mm) 2x3 CFRP plates S1012 (100x1.2 mm)
3	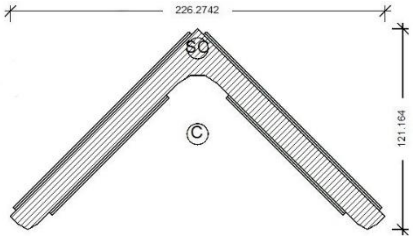	12 - 24 m	L160.15 (initial) 2x2 CFRP plates S1512 (150x1.2 mm) 2x2 CFRP plates S1012 (100x1.2 mm)
4	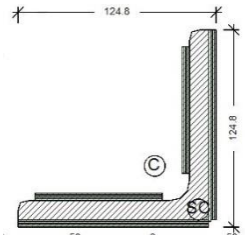	24 – 30 m	L120.12 (initial) 2x4 CFRP plates S1212 (120x1.2 mm) 2x4 CFRP plates S812 (80x1.2 mm)
5	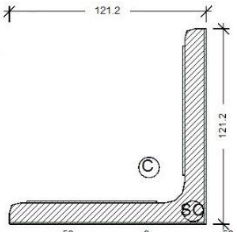	30 – 33 m	L120.12 (initial) 2x1 CFRP plates S1212 (120x1.2 mm) 2x1 CFRP plates S812 (80x1.2 mm)
6	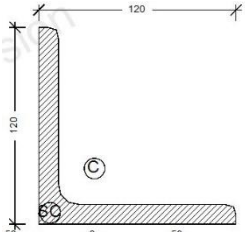	33 – 48 m	L120.12 (initial) Without CFRP plates

Table 4.3 : Brace's cross sections

No	**Braces:**	Height	Section
7	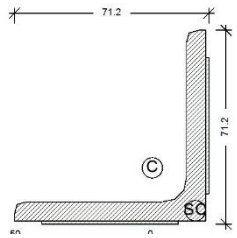	0 – 24 m and 33 – 42 m	L70.7 (initial) 2x1 CFRP plates S512 (50x1.2 mm)
8	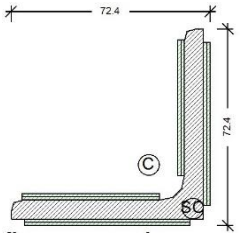	24 – 33 m	L70.7 (initial) 2x2 CFRP plates S612 (60x1.2 mm) 2x2 CFRP plates S512 (50x1.2 mm)
9	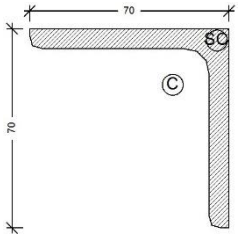	42 - 48 m	L70.7 (initial) Without CFRP plates

4.2 Modeling for Analysis

The CFRP plates are applied on the existing legs and bracings, so the reference area that is considered for the calculation of the Wind loads is equal to that of the initial tower. Actually, there is a small increase (less than 4%) which can be ignored. The self-weight of the CFRP plates can also be ignored, since it is small (less than 0.5% of the total weight of the tower).

Based on the above, it is assumed that the design loads and the load combinations of the strengthened tower are the same as the loads acting on the initial tower, which are calculated and presented in paragraph 3.2.

The strengthened members are simulated as by means of 6DOF beam elements with a new composite section, that consists of the steel section and the CFRP plates. The new composite sections of the strengthened members (legs and braces) were designed using the section designer tool of the software as shown in Table 4.2 and Table 4.3.

4.3 Global Analysis and design

At first, Modal Analysis was performed to determine the natural frequencies of the tower. The first modes and the corresponding periods are shown in Figure 3.8. Due to structure's and loads' symmetry the first two modes have the same period but refer to different (major) direction. The 3rd mode is torsional.

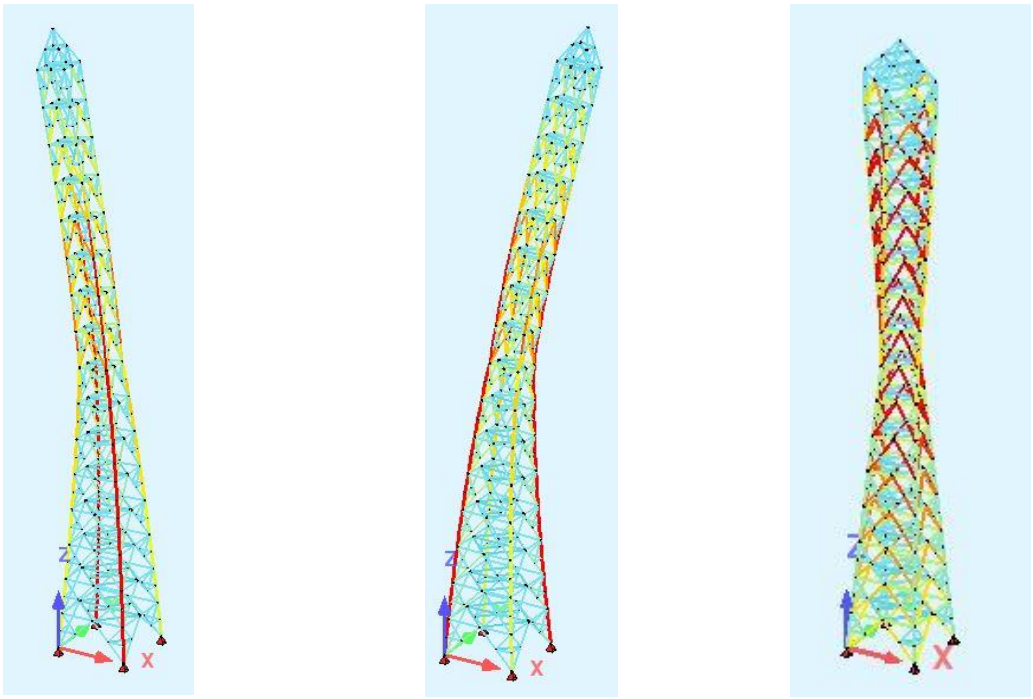

1st mode
T = 0.815 sec

2nd mode
T = 0.815 sec

3rd mode (torsional)
T = 0.23 sec

Figure 4.2: First Modes

Ultimate Limit State (ULS)

Then, 3rd order analysis was performed to verify the stability of the structure, the plasticity level and the utilization factor of each members. In 3rd order analysis, both nonlinear material and geometrical nonlinearity is taken into account. This type of analysis was used instead of linear analysis, because it is quite complicated to calculate the buckling resistance and make the relevant verifications of the strengthened members, with the new composite section (CFRP plate and angle section), in accordance with Eurocodes.

The results of the analysis are summarized below.

The maximum total utilization factor of each group of members is shown in Table 4.4.

Table 4.4: Maximum utilisation factor for members

Group of members	Maximum utilisation factor
Legs	0.991
Vertical Braces	0.967
Horizontal members	0.431
Secondary and horizontal braces	0.606
horizontal members	0.158
Horizontal braces at platform's level	0.445
Members at the top of the tower	0.063

The utilisation factor of the legs and braces along the height of the tower is shown in Figure 4.3.

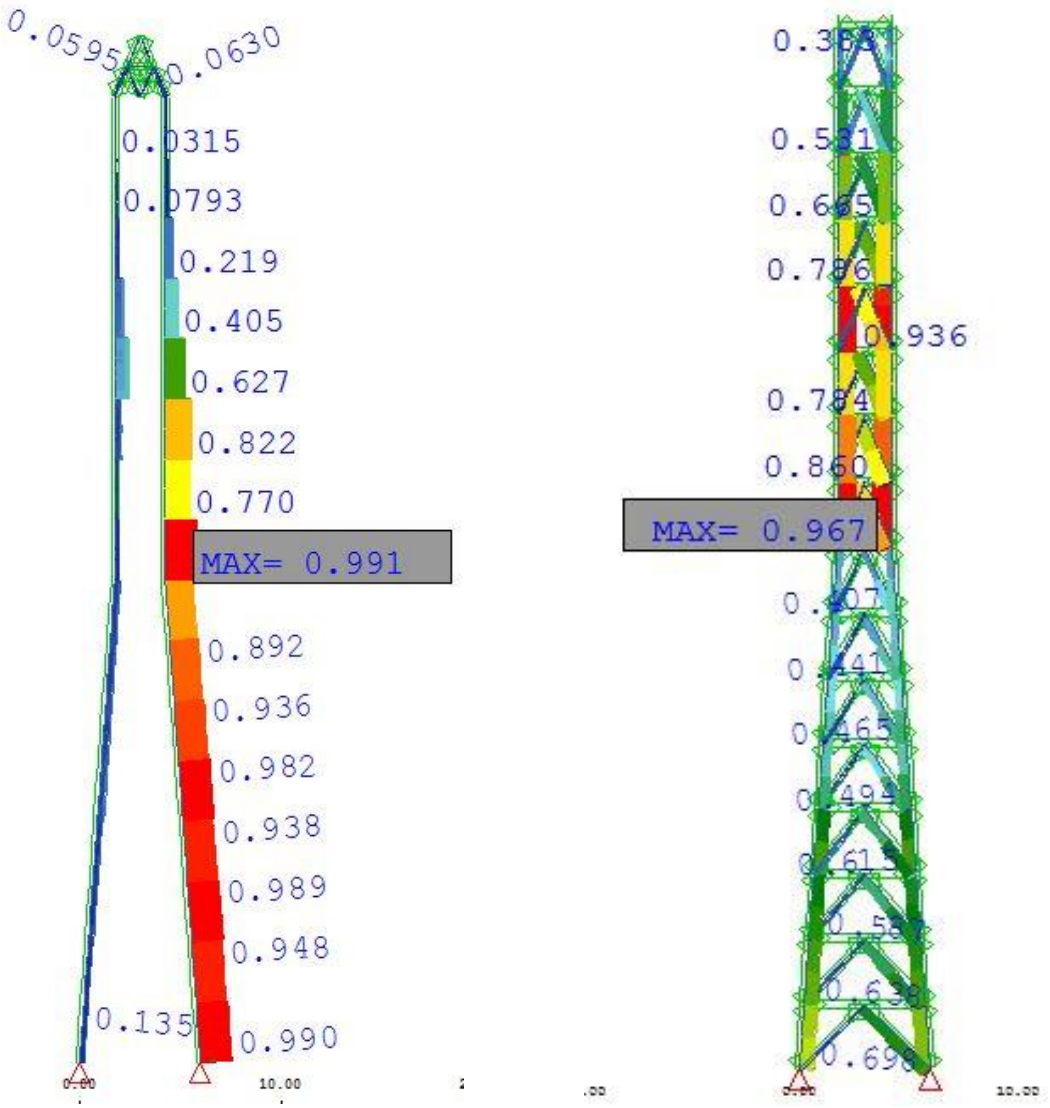

a) Legs b) Vertical Braces

Figure 4.3: Utilisation factor along the height of the tower for a) Legs and b) Braces

The maximum stresses that develop in the Leg and Brace sections are shown in Table 4.5 and Table 4.6. It is noticed that for the most unfavourable load combination the steel section yields, while the CFRP plates almost reach their compressive strength, which was considered as only 6% of-the tensile strength.

Table 4.5: Maximum stresses on steel (material 1)

Mat	Check or Criterion		Value	Limit	Unit	Level
1	Centric compression	σ-n,c	187.11	213.64	MPa	0.876
	Centric tension	σ-n,t	164.92	213.64	MPa	0.772
	Longitud. compressive stress	σ-x	249.02	213.64	MPa	1.166
	Longitud. tensile stress	σ+x	220.49	213.64	MPa	1.032
	Shear stress	τ	18.59	123.34	MPa	0.151
	Von Mises stress	σ-v	249.02	213.64	MPa	1.166
	Shear in weldings			207.85	MPa	
	Compression in compr. zone	σc-0	187.11	213.64	MPa	0.876
	Plate slenderness c/t			1.00		

Table 4.6: Maximum stresses on CFRP (material 3)

Mat	Check or Criterion		Value	Limit	Unit	Level
3	Centric compression	σ-n,c	147.01	210.00	MPa	0.700
	Centric tension	σ-n,t	129.38	2900.00	MPa	0.045
	Longitud. compressive stress	σ-x	193.97	210.00	MPa	0.924
	Longitud. tensile stress	σ+x	171.78	2900.00	MPa	0.059
	Shear stress	τ	18.00	1674.32	MPa	0.011
	Von Mises stress	σ-v	193.97	2900.00	MPa	0.067
	Shear in weldings			1488.28	MPa	
	Compression in compr. zone	σc-0	147.01	210.00	MPa	0.700
	Plate slenderness c/t			1.00		

Further on Modal Response spectrum analysis was performed to verify the member's capacity for the Earthquake load combination defined in paragraph 3.2.6**Error! Reference source not found.**. The base shear on both directions for this combination was calculated using the CQC method and is shown in Table 4.7.

Comparing the base shear for the Earthquake combination with the total lateral force that occurs for the most unfavorable wind load combinations (Table 4.8 and Table 4.9), it is noticed that it is quite smaller, so further members' verifications are omitted.

Table 4.7: Base shear for the Earthquake combination

Sum of forces (Base-Shear)

LC	H [m]	Mode	Vb X[kN]	Vb Y[kN]	Vb Z[kN]
990	base[1]	CQC[2]	133.0	3.1	0.0
991	base[1]	CQC[2]	3.1	132.8	0.0

Table 4.8: Total lateral force for the most unfavourable load combination (diagonal wind)

Sum of Loadings

Loadcase	Σ(Loads)		
	X[kN]	Y[kN]	Z[kN]
1016	255.2	255.2	-289.3

Table 4.9: Total lateral force for the most unfavourable load combination (orthogonal wind)

Sum of Loadings

Loadcase	Σ(Loads)		
	X[kN]	Y[kN]	Z[kN]
1015	0.0	302.0	-289.3

Serviceability Limit State (SLS)

Figure 4.4 shows the deformed shape of the tower, enlarged by 10 for better display, as well as the horizontal displacement at each level. The maximum displacement at the top of the tower is 397 mm, which corresponds to a vertical angle of the parabolic antennas equal to 0.57 degrees, which is accepted.

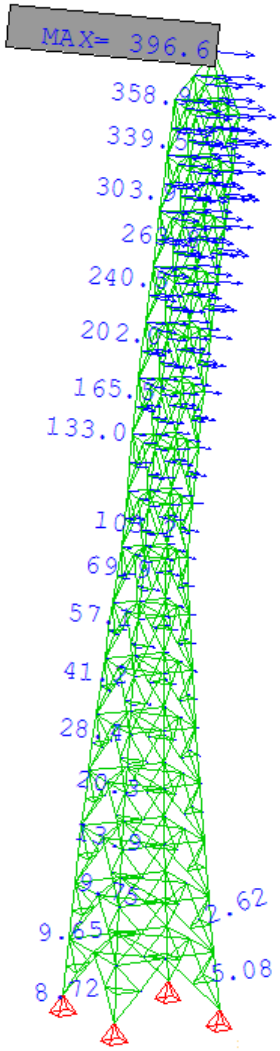

Figure 4.4: Tower's deformed shape and horizontal displacements at each level

4.4 Conclusions

This chapter addressed the design of a typical telecommunication tower strengthened with CFRP plates. Strengthening towers by using CFRP plates proved to be a possible solution, which has certain advantages comparing with the conventional strengthening method. The main advantage is that using CFRP plates there is no increase in the wind loads, since CFRP plates apply on existing members. On the other conventional strengthening method uses star battened configuration for legs and larger profiles for braces, which results in the increase of the wind loading and the self-weight of the structures.

In addition, this method of strengthening needs less time to be accomplished, less equipment and construction machinery. Therefore, it can be applied easily on mountainy and inaccessible areas in short time.

The total length of the CFRP plates that are needed is calculated and is shown in Table 4.10. The thickness of all plates is 1.2mm. Based on this, several parameters of the strengthening procedure can be estimated, such as the total cost and the total time of construction.

Table 4.10: Total length of CFRP plates

CFRP code	Width (mm)	Total Length (m)
S1512	150	132
S1212	120	54
S1012	100	132
S812	80	54
S612	60	36
S512	50	102

5 References

1. Vlachaki – Karagiannopoulou S. G. (2018). Behavior of reinforced polymers with experimental and analytical methods. Diploma Thesis, Institute of Steel Structures, National Technical University of Athens, Greece
2. ISO 527-4: Plastics: "Test conditions for isotropic and orthotropic fibre-reinforced plastic composites"
3. ASTM Designation: D 638 – 03 "Standard Test Method for Tensile Properties of Plastics"
4. ASTM Designation: D 3039/D 3039M-2002 "Standard Test Method for Tensile Properties of Polymer Matrix Composite Materials"
5. Ciupack Y. (2016) "Untersuchungen zur Bedeutung und Anwendung der Zuverlässigkeitstheorie im Bauwesen am Beispiel von Stahlklebverbindungen" PhD Thesis, Brandenburg University of Technology, Cottbus-Senftenberg, Germany
6. CNR-DT 202/2005: "Guide for the design and construction of externally bonded FRP systems for strengthening existing structures - Metallic structures", June 2007, Rome
7. Moragiannis P. I. (2015). Experimental study of steel equal-leg angles strengthened with CFRP subjected to compression and to bending. Diploma Thesis, Institute of Steel Structures, National Technical University of Athens, Greece
8. Colombi, P., Poggi, C (2006): An experimental, analytical and numerical study of the static behavior of steel beams reinforced by pultruded CFRP strips, Composites, Part B, 37 (2006) 64-63
9. Deng J., Lee M.: (2007) Behaviour under static loading of metallic beams reinforced with a bonded CFRP plate, Composite Structures 78 (2007) 232-242
10. Narmashiri, K et al (2011) Flexural strengthening of steel I-beams by using CFRP strips International Journal of Physical Sciences Vol 6 (7), 1620-1627
11. Bambach MR et al. (2008). "Axial capacity and design of thin-walled steel SHS strengthened with CFRP." Thin-Walled Structures, doi:10.1016/j.tws.2008.10.006.
12. Teng et al.(2012). "Strengthening of steel structures with fiber-reinforced polymer composites". Journal of Constructional Steel Research 78 (2012) 131–143
13. Ben et al. (2014). "Compressive Strength of Uniformly Corroded Steel Angle Members Retrofitted with CFRP." ISSN 2250-2459, ISO 9001:2008 Certified Journal, Volume 4, Issue 8, August 2014.
14. Tamai H., Hattori A., Ozawa Y., Haitani T., Takamatsu T. (2012). "Design Formula for Rehabilitated Angle Steel Member Using Carbon Fiber Reinforced Plastic Plates". 15 WCEE, Lisbon 2012